BRINE MIGRATION EXPERIMENTAL STUDIES FOR SALT REPOSITORIES

Fuel Cycle Research & Development

Prepared for

U.S. Department of Energy

Used Fuel Disposition Campaign

Florie A. Caporuscio, Hakim Boukhalfa, Michael C. Cheshire, Amy B. Jordan, and Mei Ding

Los Alamos National Laboratory

September 25, 2013

FCRD-UFD-2013-000204

Revision 2
12/20/2012

APPENDIX E
FCT DOCUMENT COVER SHEET [1]

Name/Title of Deliverable/Milestone/Revision No.	Brine Migration Experimental Studies for Salt Repositories - M2
Work Package Title and Number	Brine Migration Experimental Studies for Salt Repositories -FCRD-UFD-2013- 000204
Work Package WBS Number	M2FT-13LA0818019
Responsible Work Package Manager	Flavie A Caporuscio Flavie A Caporuscio (Name/Signature)
Date Submitted	

Quality Rigor Level for Deliverable/Milestone[2]	■ QRL-3	☐ QRL-2	☐ QRL-1 ☐ Nuclear Data	☐ Lab/Participant QA Program (no additional FCT QA requirements)

This deliverable was prepared in accordance with Los Alamos National Laboratory
(Participant/National Laboratory Name)

QA program which meets the requirements of
☐ DOE Order 414.1 ■ NQA-1-2000 ☐ Other

This Deliverable was subjected to:

☐ Technical Review
Technical Review (TR)
Review Documentation Provided
☐ Signed TR Report or,
☐ Signed TR Concurrence Sheet or,
■ Signature of TR Reviewer(s) below
Name and Signature of Reviewers
Frank Perry

☐ Peer Review
Peer Review (PR)
Review Documentation Provided
☐ Signed PR Report or,
☐ Signed PR Concurrence Sheet or,
☐ Signature of PR Reviewer(s) below

NOTE 1: *Appendix E should be filled out and submitted with the deliverable. Or, if the PICS:NE system permits, completely enter all applicable information in the PICS:NE Deliverable Form. The requirement is to ensure that all applicable information is entered either in the PICS:NE system or by using the FCT Document Cover Sheet.*

NOTE 2: *In some cases there may be a milestone where an item is being fabricated, maintenance is being performed on a facility, or a document is being issued through a formal document control process where it specifically calls out a formal review of the document. In these cases, documentation (e.g., inspection report, maintenance request, work planning package documentation or the documented review of the issued document through the document control process) of the completion of the activity, along with the Document Cover Sheet, is sufficient to demonstrate achieving the milestone. If QRL 1, 2, or 3 is not assigned, then the Lab / Participant QA Program (no additional FCT QA requirements) box must be checked, and the work is understood to be performed and any deliverable developed in conformance with the respective National Laboratory / Participant, DOE or NNSA-approved QA Program.*

SUMMARY

For the US Department of Energy Used Fuel Disposition Campaign generic repository studies we examined water content in Permian salt samples (Salado Formation) collected from the WIPP site. These samples were obtained because of ease of in-situ sample collection and known field relations. With these representative samples, we established the profile of water release and movement as a function of temperature from 30 to 275 ^{o}C. This was performed using classical gravimetric methods, which measure weight loss as a result of heating. Weight loss measured was assumed to be water. The amount of water released from salt as a result of heating was found to be correlated with the salts accessory mineral content. Gravimetric analyses of salt rich in clay and other secondary minerals lost up to 3 wt % while pure halite salt lost less than 0.5 wt % water. Water released from salt at lower temperature was reversible and is attributed to clay hydration and dehydration processes. This was confirmed by heated stage X-Ray diffraction analysis of the clay component of the salt as a function of temperature.

The analysis shows a significant loss of interlayer water in the corrensite structure between 65 and 75 ^{o}C, as indicated by the peak shifts at 13.0 to 12.6 Å and 8.64 to 8.22 Å, respectively. This interlayer water dehydration from corrensite would release 13 wt % water. No further structural changes are observed in the clay structure from 75 ^{o}C to 275 ^{o}C. However, similar examinations performed on gypsum ($CaSO_4 \cdot 2H_2O$) show that this mineral undergoes step-wise phase transformation through dehydration to produce bassanite ($CaSO_4 \cdot (H_2O)$) and then anhydrate ($CaSO_4$). The first step involves the production of bassanite at ~ 75 ^{o}C and the loss of one water molecule and the second step consists of bassanite dehydration to anhydrite beginning at a temperature of ~ 275 ^{o}C. In situ XRD analysis of gypsum transformation as a result of heating shows an abrupt phase change from gypsum to bassanite at 75 ^{o}C. At this temperature, there is some residual

gypsum in the sample due to the slow rates of gypsum to bassanite transformation. Bassanite phase stability at higher temperatures is not yet determined, but experiments are ongoing.

We examined the utilization of neutron based Filter Difference Spectrometry (FDS) to identify the nature of the water associated with salt. The results are promising and suggest that FDS could be very valuable at identify specific signatures of water associated with salt. The method may identify water signatures associated with free water, which was distinct from signatures of accessory minerals structural water present in salt. Use of FDS in situ with thermogravimetric analysis (TGA) could be a new technique to establish the quantitative evolution of water from complex salt mixtures as a function of temperature.

We also examined brine inclusion migration in single salt crystals and salt aggregates as a function of thermal gradients. The experiments examined the behavior of individual brine inclusions (one phase and two phase inclusions) in variable thermal gradients. We found that brine in both types of inclusions (liquid only inclusions and liquid/gas inclusions) was mobilized when the salt crystals were subjected to thermal gradients. Brine migrates toward the heat source in both types of inclusions. However, the gas phase in the two phase inclusions migrated away from the heat source. Brine migration occurs through a network of micron size channels created along the migration path.

We also found that at sufficiently high temperatures (T> ~160 ^{o}C) all inclusions became two-phase inclusions, in which brine migrates up the temperature gradient and the gas phase migrates down the temperature gradient. The salt dissolution / precipitation phenomena within the inclusion is controlled by a convection cell mechanism. The dissolution at the hot end of the inclusion allows the inclusion to migrate toward the heat source. The velocity of the brine migration is highly dependent on 1) the thermal gradient established across the inclusion, 2) the temperature of the hot face of the inclusion, and 3) the size of the inclusion and the chemical nature of the brine. As a result of the continued dissolution precipitation process the chemical composition of the brine changes as the brine migrates up the thermal gradient. Near the heat source the brine composition becomes dominated by NaCl whereas away from the heat source a magnesium rich salt is precipitated.

Data gained from this investigation highlights 1) the significance of the different water components associated with salt (brine inclusion, hydrous mineral structural water), 2) the temperature domains under which the water can be driven out of the salt and, 3) the parameters that affect the velocity of brine migration in salt. We determined the temperature at which clay dehydration occurs, the amount of water that can released from salt and the parameters that affect brine migration. This research highlights the need to perform experiments at larger scales to obtain quantitative data on brine migration and mineral dehydration processes representative of the components at a salt repository scale.

CONTENTS

FIGURES

TABLES

ACRONYMS

AAC Autoclaved Aerated Concrete

DTA Differential Thermal Analysis

FEHM Finite Element Heat and Mass transfer code

FDS Filter Difference Spectrometer

LANL Los Alamos National Laboratory

RH Relative Humidity

SEM scanning electron microscope

TGA Thermogravimetric Analysis

UFD Used Fuel Disposition

US DOE United States Department of Energy

WIPP Waste Isolation Pilot Plant

XRD X-ray Diffraction

BRINE MIGRATION EXPERIMENTAL STUDIES FOR SALT REPOSITORIES

1. INTRODUCTION

1.1 Objective

The United States' Department of Energy (DOE) has initiated the study of various generic options for deep geological repositories for the permanent disposition of used nuclear fuel. The exact repository concept has yet to be determined, but the U.S. has considered the possible use of Dual Purpose Canisters for storage and subsequent disposal (Greenburg and Wen 2013). These canisters can have up to 32 spent fuel assemblies (32 pressurized water reactors (32-PWR)), while many of the European concepts are limited to four spent fuel assemblies (4-PWR) (Pusch 2008; Greenburg and Wen 2013). This increased number of spent fuel assemblies will generate a greater amount of heat radiating into the host rock. Modeling suggests a 32-PWR waste package (at 60 gigawatt-days per metric ton burnup) has the potential to reach 299°C after 85 years within 1 meter from the waste package (25 years ventilation; 15 m package spacing; Greenberg and Wen 2013). These results are just one of many models or designs for a U.S. nuclear repository, and although salt repository designs would probably set a lower thermal limit, this particular model provides a bounding high temperature scenario.

The objective of the research performed consists of examining water content in rock salt and the rates and mechanisms of brine migration in salt at elevated temperatures. The experimental data obtained on salt water content and brine migration rate in a thermal gradient will be used as input to numerical models to predict the fate and transport of brine in salt. The models, in turn, will support the development of the Used Fuel Disposition (UFD) testing. Specifically we focused on the evaluation of water content in salt,

evaluation of accessory hydrous minerals associated with Salado Formation salt, evaluation of the thermal conditions necessary for the release of water from salt, and brine migration in a thermal gradient. Some of the results obtained in this study have already been incorporated into the predictive modeling developed to assess the fate of water in crushed and intact salt. The results from the experimental examination of water release from salt under an applied heat load, along with results from the hydrous mineral stability will be used in large scale models being developed to support decisions regarding waste emplacement, geometry and maximum thermal conditions.

1.2 Background

1.2.1 Water content in salt

Water content in salt varies between samples and is dependent on the salt composition and the salt deposit. Literature data report water content that varies from thousandths of wt % to several percent in bedded salt. Salt deposits containing mainly halite contain small quantities of brine distributed as small intragranular and intergranular water inclusions. The total water content is low and is usually 0.1 to 0.5 wt %. However, the water content increases significantly in samples with increased content of clays and polyhalite reaching several wt % percent in clay rich salt (Powers, 1978). Water associated with salt can occur as 1) inter-crystalline inclusions (brine pockets present in the boundaries between salt crystals and fractures), 2) intra-crystalline inclusions (brine inclusions of microns to millimeters in size within the crystals), and 3) crystal structure water within hydrous minerals present in salt such as clay, carnallite, kieserite, gypsum, and polyhalite (Figure 1) (Roedder, 1980; Roedder, 1981; Popielak, 1983). The total water content in salt and its attribution among the three components listed above is difficult to determine and there is significant variability among the data available in the literature. Variability in the data is mostly due to the difficulty of accurately measuring water content in each category and also due to sample heterogeneity (Roedder, 1981; Shefelbine, 1982). The quantity of water attributable to each one of

the major forms of water can vary significantly within samples from the same location (Hohlfelder, 1979; Hohlfelder, 1981; Hohlfelder, 1982; Shefelbine, 1982).

Inter-crystalline water occupies pores and grain boundaries and can range in size from micron size inclusions to brine pockets of many cubic meters. This can be seen when adjacent crystals are separated and the water rapidly evaporates when exposed to dry air leaving fine white efflorescences on the face of the salt crystal (Figure 1 b). Their distribution in the salt is extremely variable. Inter-crystalline water is usually released by heating of salt samples to temperatures of less than 225 ^{o}C. However, the water released under these conditions will also include adsorbed water and structural water associated with low temperature hydrated minerals (Roedder, 1981, Shefelbine, 1982).

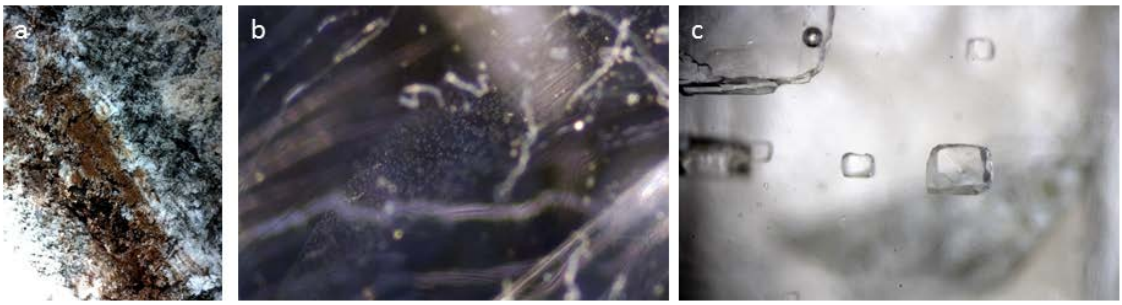

Figure 1. Picture of (a) Corrensite seam F at the WIPP repository, (b) micron size inter-crystalline water inclusions from a WIPP salt sample, and (c) mm size inclusions in a halite crystal showing both full and two phase inclusions.

Intra-crystalline water occurs as fluid inclusions that are encapsulated within single crystals. Their size can range from micron to several millimeters (Figure 1c). They are widespread in salt and can be visible to the naked eye. Smaller inclusions are easily identified by optical microscopy. Figure 2 illustrates the high density and variability of size and shapes of brine inclusions in a Salado Formation salt crystal obtained from WIPP. The inclusions can be completely filled with brine (single phase) or contain gas pockets along with brine (two phase). When heated to moderate temperatures (< 150 ^{o}C), the brine

inclusions located deeper in the salt crystals change their euhedral shape and adopt more rounded forms. Many of the smaller inclusions coalesce to create larger inclusions (Figure 1b). Intra-crystalline brine

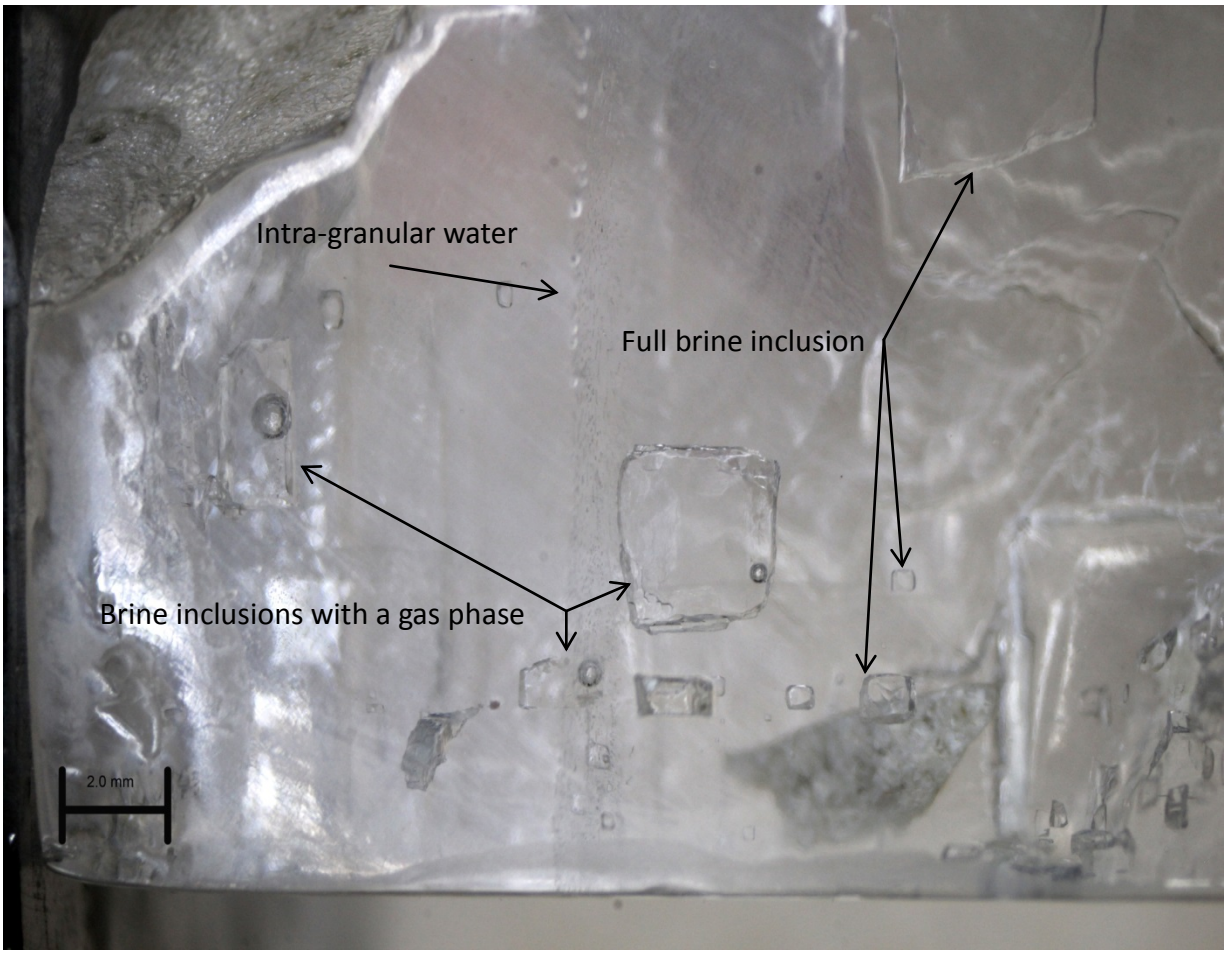

Figure 2. Image of intra-crystalline brine inclusions showing single and two-phase inclusions. Note the linear array of fluid inclusions trapped along a cleavage plane. It is possible that the original fluid was from intergranular sources that migrated to the cleavage plane and were trapped when the cleavage healed over time.

Inclusions are not readily released from salt even when heated to temperatures above 250 ^{o}C (Shefelbine, 1982). Brine contained in intra-crystalline inclusions is usually released by heating the salt to high temperatures such that the vapor pressure fractures the salt crystal. It can also be released by crushing the

salt crystal before heating, or by applying a heat gradient that causes the inclusions to move to grain boundaries. However, quantification of the water released via these processes has large uncertainties due to the size variability of the brine inclusions.

Salt deposits contain a significant amount of water associated with hydrated minerals contained in the salt. Minerals most commonly associated with salt include oxyhydroxide minerals, carnallite ($KMgCl_3 \cdot 6(H_2O)$), bischofite ($MgCl_2 \cdot 6H_2O$), kieserite ($MgSO_4 \cdot H_2O$), gypsum ($CaSO_4 \cdot 2H_2O$), polyhalite ($K_2Ca_2Mg\ (SO_4)_4 \cdot 2H_2O$) and various clay minerals. The distribution of these various hydrated minerals in salt is highly variable and varies significantly within samples from the same location (Braitsch, 1971; Stewart, 1963; Kopp and Combs,, 1975). The amount of water associated with each mineral component can be determined theoretically from their chemical formula. In a mixture of minerals, an accurate determination of the mineralogy of the sample and quantitative measurement of weight loss under thermal treatment using techniques such as differential thermal analysis (DTA) and thermal gravimetric analysis (TGA) or a combination of the two methods could in theory assign water releases to specific mineral phases. The amount of water contained in each mineral phase, its ease of release, and the potential for rehydration vary significantly between and among mineral phases. Polyhalite contains up to 6 wt % water, clay minerals can contain between 5 and 18 wt. % water and gypsum contains up to 20.9 wt % water. The first and second dehydration temperatures domains for polyhalite are 150-160 ^oC and 340 – 360 ^oC respectively. Clay minerals undergo dehydration between 100 and 800 ^oC. Gypsum undergoes dehydration between 75 to 175 ^oC. Carnallite, a secondary mineral phase often associated with salt containing up to 38.9 wt % water undergoes dehydration between 180 and 224 ^oC (Freyer and Voigt, 2003). These examples show the range of water contained in mineral phases associated with salt and the temperature domains at which many of these phases undergo dehydration. Not only do these dehydration temperature domains overlap, there are also kinetic effects that slow reactions, thus increasing the difficulty of assigning TGA data to the various minerals and highlighting the importance of accurate quantification of water content and dehydration reaction conditions using site-specific trace minerals.

The constituents found in brine have been examined in the literature and a number of synthetic analogues have been proposed as model brines from the different brines that might come in contact with nuclear waste (Brush, 1990; Snider, 2003). Compositions of natural brines were determined by analysis of seeps collected in the Duval potash mine, N.M. and by analysis of micro liter samples extracted from fluid inclusions (Dosch, 1976; Molecke, 1983). Synthetic analogs of this composition labeled Brine A (Table 1) was utilized in numerous studies that were intended to mimic the Duval mine brine. The composition of Brine A is different from the composition of brine obtained by dissolving WIPP salt in distilled water (Brine B, Table 1). These model brine solutions were later replaced by ERDA-6 (replaced Brine B) (Brush, 1990) and GWB (replaced Brine A) (Snider, 2003) in laboratory and modeling studies used for WIPP performance assessment. The synthetic ERDA-6 is designed to represent fluids in brine reservoirs in the underlying Castile Fm. (Popielak, 1983) and GWB is designed to represent the average composition of inter-granular brine fluids obtained through numerous analyses of inter-granular fluids obtained through different studies of WIPP salt specimens.

Table 1. Constituents of brine samples from the Duval mine and synthetic WIPP brines. Concentrations are in g/L for all constituents (Brush, 1990, Snider, 2003).

Constituent	Duval mine	Brine inclusions	WIPP Brine A	WIPP Brine B	GWB	ERDA-6
Na^+	49	33	42	115	81	112
K^+	52.5	26	30	0.015	18	3.8
Mg^{2+}	38.5	43	35	0.01	24.8	0.46
Ca^{2+}	1.26	5.5	0.6	0.9	0.56	0.48
Sr^{2+}	-	-	0.005	0.015	-	-

Cl^-	241.5	241	190	175	208	170
SO_4^{2-}	3.6	-	3.5	3.5	-	-
I^-	-	--	0.01	0.01	-	-
HCO_3^-	0.7	-	0.7	0.01	-	-
Br^-	0.385	-	0.4	0.4	2.12	0.88
HO_3^-	1.16	-	1.2	0.01	-	-
TDS	388	350	306	297	-	-

Brine inclusions are typically enriched in potassium and magnesium and relatively poor in calcium (Table 1). The origin of these fluids inclusions trapped within the halite crystals is the original brine in which the ionic ratios between Ca, Mg and SO_4 were influenced by the reaction of brine with carbonates adjacent to the halite beds and the dissolution of efflorescent evaporate crusts that were not in equilibrium with precipitated evaporates (Bein, 1991, Brush 2012).

1.2.2 Brine migration under temperature gradients

Extensive studies examined brine migration in salt at scales ranging from cm to meters in the laboratory and under real mine settings (Machiels, 1981; Yagnik, 1982; Yagnik, 1983; Bradshaw, 1971; Krause, 1983; Nowak, 1986; Nowak, 1987; Rothfuchs, 1988). Under the influence of temperature gradients, water/brine contained in the grain boundaries (inter-granular) is released by a vapor transport process. This process is facilitated by the opening of the grain boundaries in polycrystalline natural salt due to the thermal stresses which accompany the thermal gradients applied to the salt (Machiels, 1981).

Intra-granular water migration in a temperature gradient depends on the nature of the brine inclusion. All-liquid brine inclusions within salt crystals migrate up the temperature gradient according to a mechanism

controlled by the rate of salt dissolution at the hot face of the inclusions and to a lesser extent on the rate of salt crystallization at the cold face of the inclusion (Olander, 1980; Olander; 1981a; Olander, 1981b, Roedder, 1980). Inclusions are predicted to move towards the heat source because of the temperature effect on the solubility of salt. Salt will dissolve at the interface closest to the heat source and precipitate at the interface furthest from the heat source because salt solubility increases with increasing temperature (Machiels, 1981, Yagnik, 1982, Yagnik, 1983). This process is highly dependent on the presence of imperfections and impurities in the crystal structure. A dissolution front with imperfections in which the atoms of the solid salt are less tightly bound than in a perfect atomic plane will dissolve faster (Machiels, 1981). The rate of inclusion transport is dependent on the nature of the salt and the presence of impurities, and to a lesser extent, on the rate of ion diffusion through the brine droplet, and the precipitation of salt at the cold side of the salt.

Brine inclusions containing a gas phase will move away from the heat source because water will evaporate at the hot side of the gas bubble and move to the colder side of the inclusion and condense. This mechanism will create an internal flow that continually brings dissolved salt from the cooler side of the inclusion to the hot side of the inclusion and water vapors from the hot side of the inclusion to the cooler side of the inclusion. This flow and evaporation mechanisms will induce the gas-liquid inclusions to move away from the heat source (Anthony, 1972; Olander; 1981a; Olander, 1981b).

The behavior of all liquid and gas-liquid inclusions becomes complicated when the inclusions reach grain boundaries, or deposits of secondary minerals associated with salt. In some studies, the migration of the inclusions was reported to continue within the adjacent grain and in other cases it ceases and the fluid spreads into micro-cracks at the boundary between grains (Roedder, 1980). The behaviors of brine inclusions that accumulate at grain boundaries and inter-crystalline brine are basically unknown. It is also unknown how the presence of secondary mineral phases such as gypsum, polyhalite and clay affect brine migration. Multi-scale laboratory and field studies are essential to investigate knowledge gaps in

individual processes and integrate the knowledge gained at a small scale (0.1 to 10 cm) to interpret larger scale in-situ testing studies.

1.3 Secondary minerals associated with Salado Formation salt and their hydration/dehydration properties

1.3.1 Accessory minerals associated with Salado Formation salt at WIPP.

The WIPP repository is located within the Salado Formation, which consists primarily of halite, with minor amounts of anhydrate, polyhalite, gypsum, mangnesite, quartz, clays, and trace amounts of K-feldspar (Krumhansl, et al, 1990). The total content of secondary minerals in the WIPP repository horizon is approximately 5 wt % (Stein, 1985). Clays occur either as discrete layers with thicknesses ranging from a few to several cm (Figure 3), or as finely dispersed material throughout the halite. Characterization by X-ray diffraction identified three main clay minerals (mixed-layer saponite-chlorite, chlorite, and illite) as the bulk of the argillaceous material comprised in the salt. This is consistent with clay minerals common to many other salt bed formations typically consisting of illite and an assortment of Mg-rich poorly-ordered, randomly-interstratified clays (Braitsch, 1971). The X-ray spectra vary significantly between samples suggesting either variation in the relative proportions of the trioctahedral chlorite and trioctahedral smectite layers or the lack of ordering between the chlorite and smectite layers.

Figure 3. Picture of the clay (corrensite) seam F in the newly excavated SDI rooms E690N500-N350. The clay-bearing strata do not show any significant systematic mineralogical variations. Within any given layer the proportions of the three clays appear to vary randomly from place to place except for the apparent enrichment of mixed-layer in the upper clay compared to the lower clay. The mixed-layer/illite and mixed-layer/chlorite ratios appear to be higher in the upper clay, while the illite/chlorite ratio shows no trend.

Sulfate minerals associated with salt have been examined to determine their ability to retain and release significant amounts of water through hydration/dehydration processes as a function of heat and pressure loads. The gypsum ($CaSO_4 \cdot 2H_2O$) to anhydrite transformation creates a large water release (up to 21% wt. loss) and volume reduction (of up to 40%) (Smyth and Bish, 1988). Sulfate volume loss results in

contraction, which can affect salt porosity by creation of fractures. In addition to gypsum, hydrated minerals (sulfates, chlorates) most commonly associated with salt (other than clays) include carnallite ($KMgCl_3 \cdot 6(H_2O)$), bischofite ($MgCl_2 \cdot 6H_2O$), kieserite ($MgSO_4 \cdot H_2O$), and polyhalite ($K_2Ca_2Mg(SO_4)_4 \cdot 2H_2O$). The distribution of these various hydrated minerals and the water associated with them is highly variable and varies significantly within samples from the same location (Braitsch, 1971, Stewart, 1963, Kopp and Combs, 1975). Calcium sulfates are classified in three different mineral forms based on their degree of hydration. The phase changes of the calcium sulfates are: gypsum ($CaSO_4 \cdot 2H_2O$), hemihydrate (or bassanite) ($CaSO_4 \cdot 0.5H_2O$), and anhydrite ($CaSO_4$). The phase transformations occur naturally through dehydration processes but are accelerated following heat treatments. Phase transformations are influenced by the amount of water present, the temperature, pressure, and amount of dissolved electrolytes or organics (Freyer and Voigt, 2003).

1.3.2 Clay stability and hydration/dehydration properties

A number of previous studies examined the changes in smectite clay at elevated temperatures and/or pressures Altaner and Ylagan (1997) provide a good introduction to the concepts of smectite alteration. Smectite illitization is considered to proceed through mixed-layer illite/smectite (I/S) intermediates as the percentage of illite interlayer increases. Important factors for the changes include increasing temperature, potassium (K) concentration, time, and water/rock ratio. Possible reaction mechanisms for smectite illitization include solid-state transformation, dissolution and crystallization, and Ostwald ripening. Wu and colleagues (Wu et al. 1997) examined partial dehydrated Ca- and Mg-exchanged montmorillonite by heating samples at pressures from the H_2O liquid-vapor boundary to about 10 kbars. Progressive dehydration caused shrinkage of the crystal lattice from the 19 Å hydration state to the 15 Å at 260-350 ºC with further dehydration to the 12.5 Å state at higher temperature. Mg-montmorillonite dehydrates to the 15 Å state at 200-250 ºC, with further dehydration to the 12.5 Å state at 590-605 ºC. Similar experiments with Na-exchanged montmorillonite (Huang, 1994) identified shrinkage from the 19 Å hydration state to the 15 Å hydration state at 330-385 ºC and from 15 Å to 12.5 Å at 485-500 ºC. The 19

Å fully hydrated montmorillonite therefore, is stable up to 200-380 ºC under pressures in the absence of potassium..

Ferrage et al. (2011) presented some of the best evidence for the mechanism of S to I/S transformation. They studied the hydrothermal reactivity of K-exchanged low-charge montmorillonite (SWy-2) at 250-400 °C and 1 kbar, with reaction times of 5 to 120 days. The authors provide experimental evidence for a dissolution-crystallization mechanism following the Ostwald step rule in which metastable smectite transforms into illite through a series of metastable illite-smectite phases. Dehydration and lattice shrinkage that occurs in this temperature range is fully or almost fully reversible. However, at higher pressures, the rehydration initially follows a lower-temperature path relative to the thermal path of dehydration.

The effect of dehydration was examined at 250, 500, and 650 ^{o}C by treating the samples for 1 hour at the designated temperatures (Krumhansl, 1990). The results show significant structural alterations as a result of the heat treatment. The peaks characterizing the chlorite and corrensite are significantly reduced by the heating process. However, the illite peak remains prominent throughout the various heat treatments examined (Krumhansl, 1990).

1.3.3 Sulfate minerals dehydration properties

Hydration/dehydration of calcium sulfates have been studied extensively in relation to their utilization as binders in building materials (Freyer and Voigt, 2003). At low temperature gypsum is the most stable phase and at high temperature anhydrate is the most stable mineral form. Hemihydrate is metastable at all temperatures. Gypsum/anhydrite transition temperatures are in the range of 25 to 52 ^{o}C (Freyer and Voigt, 2003). However, gypsum ($CaSO_4 \cdot 2H_2O$) also converts to anhydrite ($CaSO_4$) in evaporite beds between the temperatures of 100 and 140 ^{o}C. In that 40 ^{o}C gap is hemihydrate, a metastable but kinetically favored phase (Shcherban and Shirokikh, 1971). The more stable phase with the same chemical formula as hemihydrate is termed bassanite. These transition temperatures are strongly

influenced by electrolytes. Increased electrolyte influences the solubility domains of each mineral phase and their transition temperatures. In a solution saturated with NaCl the transition temperature for the gypsum/anhydrite is estimated to 18 ^{o}C (Hardie, 1967, D'Ans, et al 1955), and the transition of gypsum/hemihydrate estimated to 76 ^{o}C (Freyer, 2000). Increased pressure increases the solubility of all calcium phases and also influences the transition between the different phases. Solubility increases as a function of pressure for the different phases and shifts the phase transition temperatures of gypsum/anhydrate and gypsum/hemihydrate. However, only a few reports based on thermodynamics exist on calcium sulfate phase transition as a function of pressure (Monnin, 1990, Monnin, 1999, Krumgalz et al 1999).

Dehydration of carnallite occurs in the 80 ^{o}C to 170 ^{o}C and results in the release of 3 to 8 wt % water. A second dehydration stage occurs at much higher temperatures to produce a mixture of magnesium chloride and magnesium oxide. The dehydration of bischofite occurs between 155 to 220 ^{o}C. Recent examinations of bischofite dehydration in the temperature range 25 ^{o}C to 600 ^{o}C using high-quality in situ synchrotron powder diffraction data identified at least eight phases including: $MgCl_2 \cdot nH_2O$ (n = 1, 2, 4 and 6), $MgOHCl \cdot nH_2O$ ($0 \leq n \leq 1.0$), $MgCl_2$ and MgO (Sugimoto, 2007).

Polyhalite minerals, which possibly formed as a result of the reaction of brine with gypsum or anhydrate, are described as a tipple salt and are represented by the formula ($K_2 SO_4 \cdot MgSO_4 \cdot 2Ca SO_4 \cdot 2H_2O$). It is the most wide spread sulfate mineral in evaporatic rock salt formations and can be present in Salado Formation salt up to 5 wt %. The formation of polyhalite minerals may be the result of the reaction of brine with gypsum or anhydrite. The hydrate water is coordinated to the magnesium ion and therefore is only released at temperatures above 250 ^{o}C. The loss of water from salt between 280 ^{o}C and 360 ^{o}C is typically attributed to the dehydration of polyhalite.

2. METHODS AND EXPERIMENTAL DESIGN

2.1 WIPP salt sampling and sample preservation

Salt samples used in our experiments were collected at the WIPP underground salt mine. The clay rich samples were collected from clay seam F in the freshly excavated rooms (SDI, E690N500-N350). Salt samples from the orange marker bed were also collected at the same location (Figure 4). The clay component of the salt had a grey to brown appearance and was saturated with water. The salt samples collected were immediately transferred to plastic containers and sealed to preserve the salts moisture content. Samples of pure halite were also collected in panel 7. The pure halite salt samples had larger crystals and contained less accessory minerals. All salt samples were repackaged after exiting the mine. The clay rich samples were transferred to plastic bags and were sealed using a thermal heater sealer, and then were put back in the plastic containers and tightly sealed with a lid until used.

Figure 4. Picture of the clay rich zone in orange marker bed in the newly excavated SDI rooms E690N500-N350.

2.2 Rock salt water content characterization

We examined water and accessory minerals content in rock salt samples collected from the underground salt mine at WIPP by measuring loss of weight as a result of heating. We assumed that all weight loss measured was due to water loss. The samples examined in this study were collected from the clays seam F, the orange marker bed (Figure 4), and pure halite bed in the newly excavated rooms (SDI, E690N500-N350). Samples were weighed, subjected to the desired temperature and weighed again until they reached a constant weight at the designated temperature. A total of thirteen samples with individual weight ranging from 100 to 200 g were used in determining water content at the different temperatures. Weighing of the samples was performed every 8 to 12 hours and total heating duration at each temperature was typically 24 to 72 hours. The dehydration experiments were performed in a heating oven equipped with exhaust vales that allow the control of the oven vacuum. The samples were gradually heated to 65 ^{o}C, 110 ^{o}C and 265 ^{o}C respectively. The maximum vacuum applied was 15 mmHg at 265 ^{o}C to insure the release of all water associated with the rock salt. The moisture released from these experiments was not collected. In a separate experiment we connected the heating oven to a vacuum trap cooled with crushed ice and collect the condensates released from the salt. Although some water was collected in the trap, its mass was significantly less than the weight loss recorded for the salt.

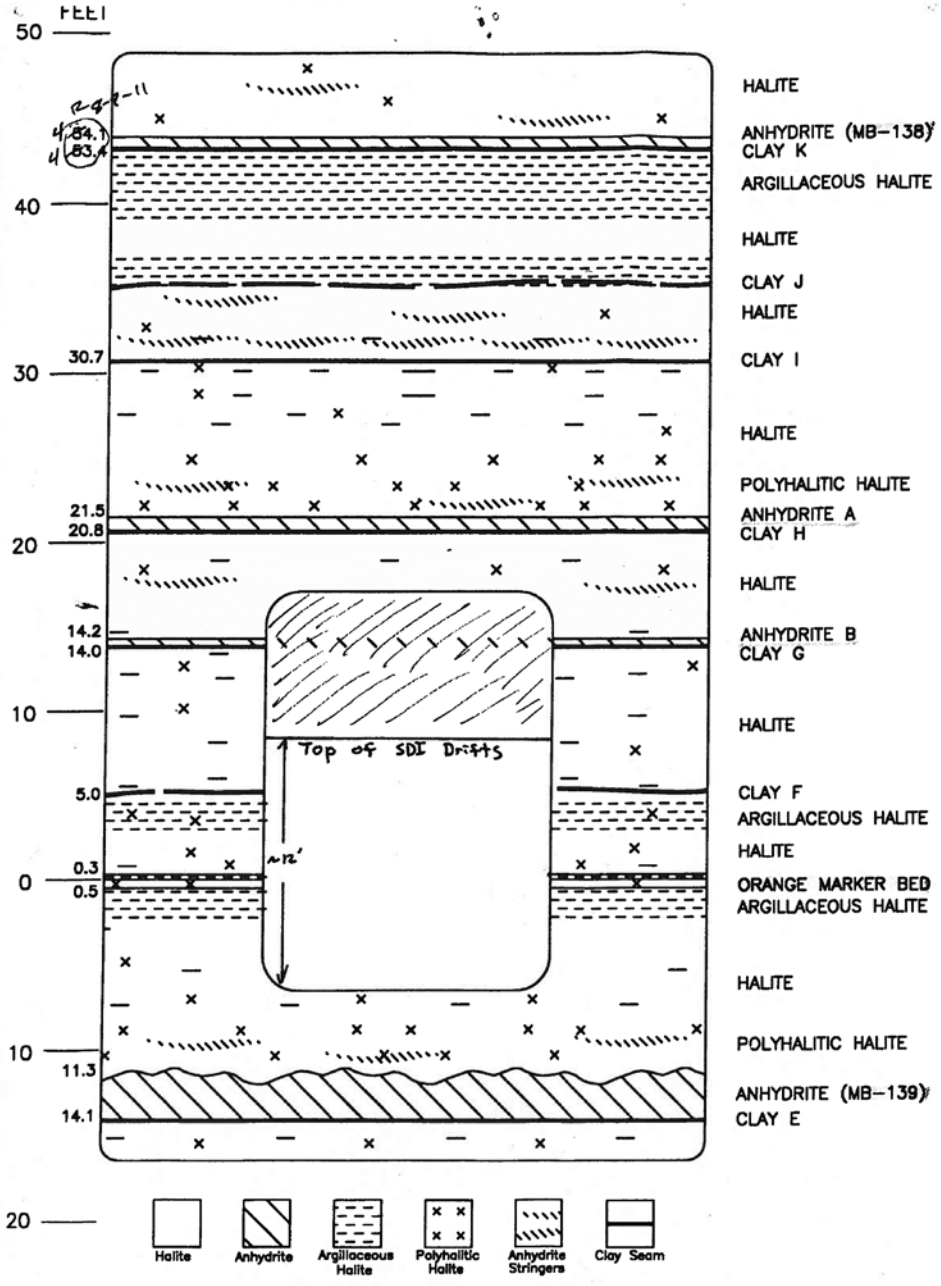

Figure 5. Schematic of the WIPP underground mine stratigraphy [DOE/WIPP 02-3177].

2.3 Characterization of crushed salt porosity

Crushed salt porosity was determined for salt samples collected from the underground mine at WIPP. The samples were a mixture of salt containing fine grains and blocks of salt of few centimeters. The salt used

for these experiments was not preserved for moisture content control and was used as collected from the mine. The salt was transferred to a large 5 L beaker until the salt reached the 3.5 L mark. Saturated brine was added to the crushed salt in successive additions. The volume of each addition and volume of liquid increase in salt were recorded. The porosity of the salt was determined as a ratio of the volume of the brine added over the volume of brine increase in the crushed salt.

2.4 Characterization of accessory mineral associated with salt using X-ray diffraction spectroscopy

X-ray diffraction (XRD) analyses were conducted on bulk salt samples, clay purified from clay Seam F, accessory minerals from the orange maker bed, and gypsum. The samples used for bulk analyses were ground and homogenized before the analysis. Analysis of the clay component of the salt was performed on clay separated from the rock salt by dissolution of the salt component. The samples were ground and suspended in DI water to drive the dissolution of salt. The supernatant was removed after saturation and replaced with fresh DI water. The operation was repeated until the clay remained suspended in solution for an extended time. The clay fraction was collected by centrifugation and was dried in an oven at 90 ^{o}C. X-ray diffraction (XRD) analyses were performed on a Siemens D500 diffractometer using Cu-Kα radiation. Data were collected from 2 to 70 °2θ with a 0.02 º2θ step-size and count times of 8 to 12 seconds per step. An aliquot of the < 2 μm suspension was dropped on an aluminum sample mount or a zero-background quartz plate and dried. This oriented mount was X-rayed from 2 to 40 °2θ at 8 to 12 s per step. Mineral identification and unit-cell parameters analysis was performed using Jade© 7.5 X-ray data evaluation program with ICDD PDF-4 database. Quantitative phase analysis was performed using FULLPAT (Chipera and Bish, 2002).

Clay and gypsum dehydration phase transitions were performed using in situ X-ray diffraction characterization under controlled temperature and relative humidity. We used a Siemens D500 diffractometer equipped with an environmental cell (Figure 6) connected to a humidity generator which allows for XRD measurements to be performed under controlled conditions of RH and temperature. The sample holder is equipped with a heating stage and an external temperature controller which accurately maintains temperature of the sample with +/- 0.5 ^{o}C. We used this experimental setup to characterize the structural changes in the clay and gypsum under equilibrium conditions at 10 to 35 % RH and variable temperature conditions varied from 25 ^{o}C to 275 ^{o}C.

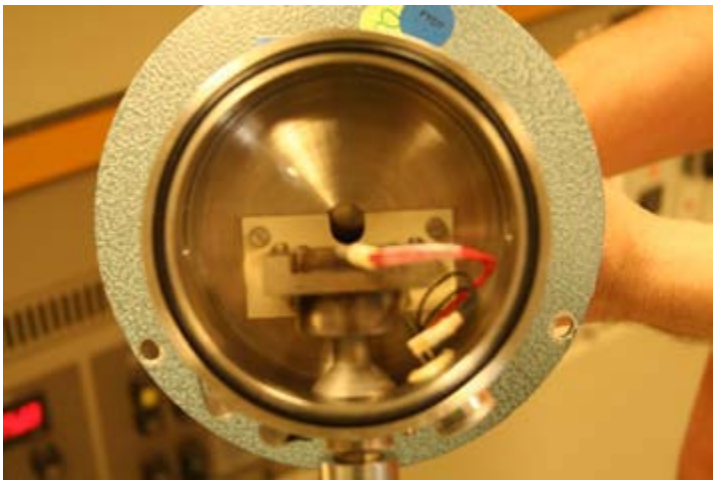

Figure 6. Anton Paar TTK 300 X-ray diffractometer environmental cell. This XRD cell was used for in situ XRD examination under controlled temperature and relative humidity.

Gypsum mineral stability experimental runs were performed for 6 weeks at 300^{o}C and 150 bar using Dickson rocking autoclaves (Figure 7). Low overall sulfate abundances in the Salado Formation horizons of interest necessitated the use of gypsum samples from Mexico for the phase stability studies. The reactants (DI water, Naica Mexico gypsum) were loaded into gold tubing, welded (Figure 8), and inserted into a 500 ml Gasket Confined Closure reactor (Seyfried et al. 1987). Experiments were then pressurized to 150 - 160 bar and were heated isothermally at 300 °C for 6 weeks. Post experiment reactants were then characterized by XRD for final mineral characterization.

Figure 7. Bridgeman seal-type pressure vessel for 300°C, 150 bar hydrothermal experiment

Figure 8. Examples of gold capsules prepared for high temperature, pressure (300 °C, 150 bar) experimental sulfate runs.

2.5 Characterization of water associated with salt using filter difference spectrometer (FDS)

FDS is vibrational spectroscopy technique that uses inelastic incoherent neutron scattering to characterize phenomena such as the motion of atoms (i.e., rotational mode, molecular vibration). This technique is very sensitive to vibrational modes of water and can discriminate between free and bound water. The neutron scattering intensity is extremely sensitive to the amplitude of the librational mode motion and therefore very sensitive to the molecular environment of water (hydrogen-bonding, surface, binding to cations) which influences water motion. Examination of water vibrational signature is a powerful tool to

investigate the nature of water in materials. It is well suited to fingerprint different types of waters in geological materials, (e.g., structural water, bulk water, and surface water) (Line and Kearley, 2000). It is used here for the first time to investigate the form of water in bulk salt samples from WIPP.

2.6 Salt characterization using thermogravimetric analysis (TGA)

TGA is commonly used to determine selected characteristics of materials that exhibit either mass loss or gain due to decomposition, oxidation, or loss of volatiles such as moisture. In this study, we used TGA to determine weight loss of water in samples as a result of heating.

2.7 Scanning electron microscope analysis of salt samples used in brine migration studies

SEM analyses were performed on salt efflorescence collected at the surface of salt crystals subjected to thermal treatments and on salt crystals sectioned along the brine migration pathways. The analyses were performed with an FEI™ Inspect F scanning electron microscope (SEM). The samples were carbon coated prior to the analyses. Imaging with the SEM was performed using a 5.0 to 10.0 kV accelerating voltage and a spot size of 1.5 to 3.0. Energy dispersive X-ray spectroscopy (EDX) used to perform elemental analyses of selected salt features was performed at 30 kV and a 3.0 spot size.

2.8 Brine migration in intact salt as a function of temperature

Brine inclusion migration in salt crystals were examined using a custom built setup which consisted of a heating stage, an optical microscope equipped with a digital camera, and a temperature controller (Figure 9). The salt crystals are sandwiched between two aluminum blocks adjusted by a screw drive. The first aluminum block is heated by an OMEGA heater fire rod with 250 W built directly into the aluminum block. The temperature of the heating block is controlled by a thermocouple and a temperature controller (J-KEM scientific model 210) that maintains the temperature with ± 2 ^{o}C of the designated temperature.

The second aluminum block is not heated and equilibrates to slightly above ambient temperatures. The heating stage is mounted on Autoclaved Aerated Concrete (AAC) insulator blocks. Images of the salt crystals are captured with an Olympus digital camera D70 or a canon SLR camera coupled to the optical microscope. Images are captured automatically for the duration of the experiment at selected time intervals. Transformation and migration of the inclusions is determined by analyzing the successive images captured over time. All image processing was performed using Photoshop and videos were processed using the software VirtualDub an open-source video capturing and processing utility http://virtualdub.optimumdownloader.com.

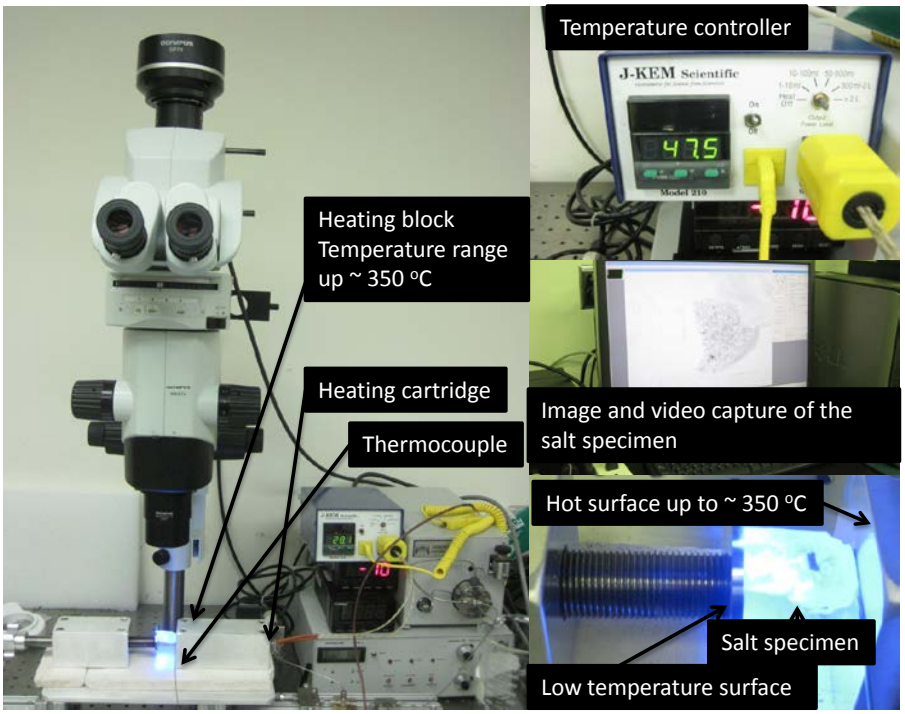

Figure 9. Temperature controlled heating stage and microscopy used for the inclusion migration studies

3. RESULTS AND DISCUSSION

3.1 Characterization of rock salt from the WIPP underground mine

3.1.1 Characterization of total water content in WIPP salt samples

Accurate determination of water content in salt is difficult to obtain. Water is present in rock salt associated with accessory minerals, adsorbed to the salt surface, or as discrete inclusions distributed throughout the salt. Obtaining an accurate measurement of each fraction is quite difficult because of the constant changing of the samples during their preparation for the experiment. Water evaporation, rapid dehydration/rehydration of accessory minerals, and loss of moisture during salt disaggregation can cause significant variations in water content determination. In addition, water content in salt is very heterogeneous and changes significantly based on the sampling location and the type of samples collected. Other uncertainties arise from the sampling and sample preservation. This study targeted determination of total water content in salt samples collected from clay seam F, and the orange marker bed (see methods for more details on sampling and sample preservation). The experiments were performed by heating salt samples and recording their weight loss. Weight loss at all temperatures was assumed to be water. The weight loss was recorded every 8 to 12 hours until their weight was constant. The dehydration experiment was performed at 65, 110, 165, and 265 ^{o}C. The plot in Figure 10 shows the weight loss for individual salt samples as a function of temperature and heating duration.

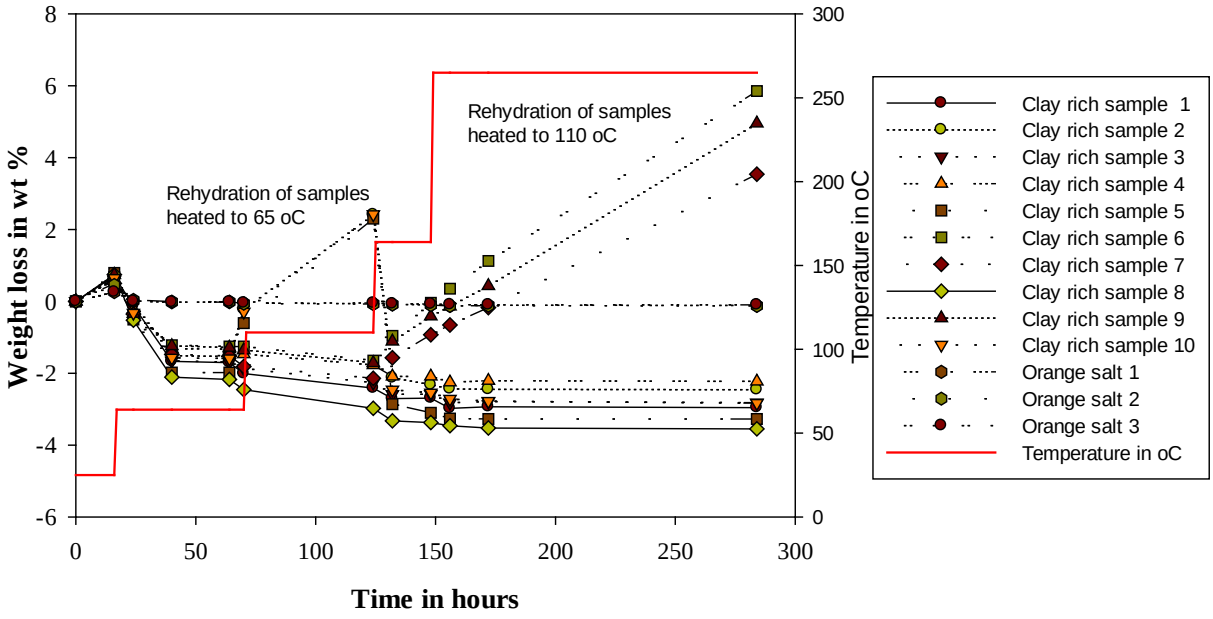

Figure 10. Plot of salt weight loss as a function of time for a series of 13 salt samples with different accessory mineral content. The salt samples were collected from WIPP and used with minimal desegregation. Rehydration of samples heated at 65 ^{o}C shows the weight gain for samples removed after equilibration at 65 ^{o}C and placed in a humid environment at room temperature. Rehydration of samples heated at 110 ^{o}C shows the weight gain for samples removed after equilibration at 110 ^{o}C and placed in a humid environment at room temperature.

The initial weight gain, which ranged between 0.1 to 0.8 wt % for all samples was due to moisture absorption from the moist air during the sample's equilibration at room temperature before the start of dehydration experiment. Heating at 65 ^{o}C results in a weight loss of 0.1 to 2 wt %. The clay-rich samples lost the largest amount of water. The samples from the orange marker bed lost less than 0.25 wt% of their total weight. The dehydration of the clay rich samples at 65 ^{o}C was reversible. Three samples removed from the oven and equilibrated in a moist chamber recovered rapidly their weight and continued to accumulate water rapidly (Figure 10).

At higher temperatures all samples continued to lose weight. The samples rich in clay and other accessory minerals lost the largest amount of moisture at higher temperatures. The dehydration process is also reversible for all samples heated for up to 165 ^{o}C, as is shown in figure 10. Samples removed from the

dehydration experiment at 165 ^{o}C and placed in a moist environment rapidly recovered all the moisture lost and continued to accumulate moisture far beyond their original moisture content. This is an indication that the transformations observed are reversible and that the accessory mineral associated with salt are dominated by clay which can undergo reversible hydration/dehydration processes. However, some irreversible transformations and contribution from other mineral phases could be occurring in the sample but are hard to detect because of the large amount of clay. More detailed examinations are needed to determine the different minerals that are associated with salt and their individual behavior with regard to hydration/dehydration processes. However, it is clear from our initial data that clay and other secondary minerals content control the amount of moisture accumulated and released by rock salt. This is evidenced by the correlation between the amount of moisture released by the samples and their accessory mineral content Figure 11.

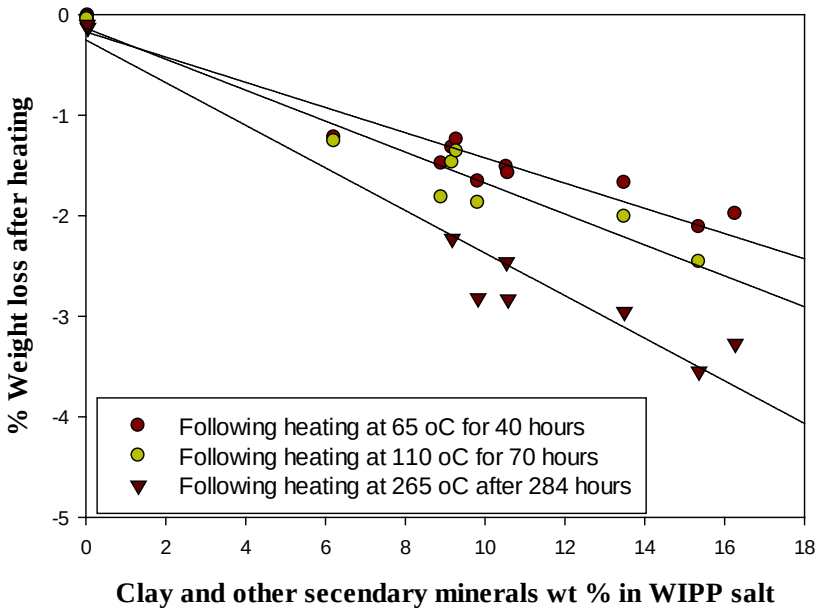

Figure 11. Weight loss as a function of temperature and heating duration for salt samples collected from WIPP. Samples with high secondary mineral content were collected from clay seam F and the samples with low secondary mineral content were from the orange marker bed.

The data in figure11 show a linear correlation between the total weight loss of the samples at a given temperature as a function of the sample's accessory minerals content. The three samples with the lowest clay content from the orange marker bed had the lowest water loss. All other samples collected near the clay seam F had significantly more accessory minerals and significantly more water content. The average weight loss of the rock salt from clay seam F at the different temperatures examined is shown in Table 2.

Table 2. Average weight loss as function of the heating temperature for samples from Clay seam F and Orange marker bed.

Sample description	**Average weight loss at 65 ^{o}C in wt%**	**Average weight loss at 110 ^{o}C in wt%**	**Average weight loss at 265 ^{o}C in wt%**
Rock salt from clay seam F	1.57 ± 0.30	1.63 ± 0.42	2.87 ± 0.45
Orange marker bed	0.016 ± 0.01	0.054 ± 0.01	0.12 ± 0.01

The data clearly show that accessory minerals control the release of moisture from rock salt under the influence of temperature.

The residual minerals were from the samples heated to 65 oC were dried in the oven at 65 ^{o}C until they retained a constant weight and were analyzed by X-ray diffraction (Figure 12 and 13). All samples examined had significant amounts of clay rich phases. Residues from clay seam F salt were composed of primarily corrensite with minor amounts of quartz, magnesite, mica, kaolinite (or possibly chlorite), hematite, and anhydrite. The residues from the heated orange marker bed were composed of primarily corrensite with minor amounts of quartz, magnesite, mica, kaolinite or possibly chlorite, hematite, and anhydrite. All samples contained residual halite. The data support the observations from the heating experiments that show that most of the weight loss was observed at T < 110 ^{o}C was reversible and is

consistent with the temperature realm under which corrensite undergoes hydration/dehydration processes.

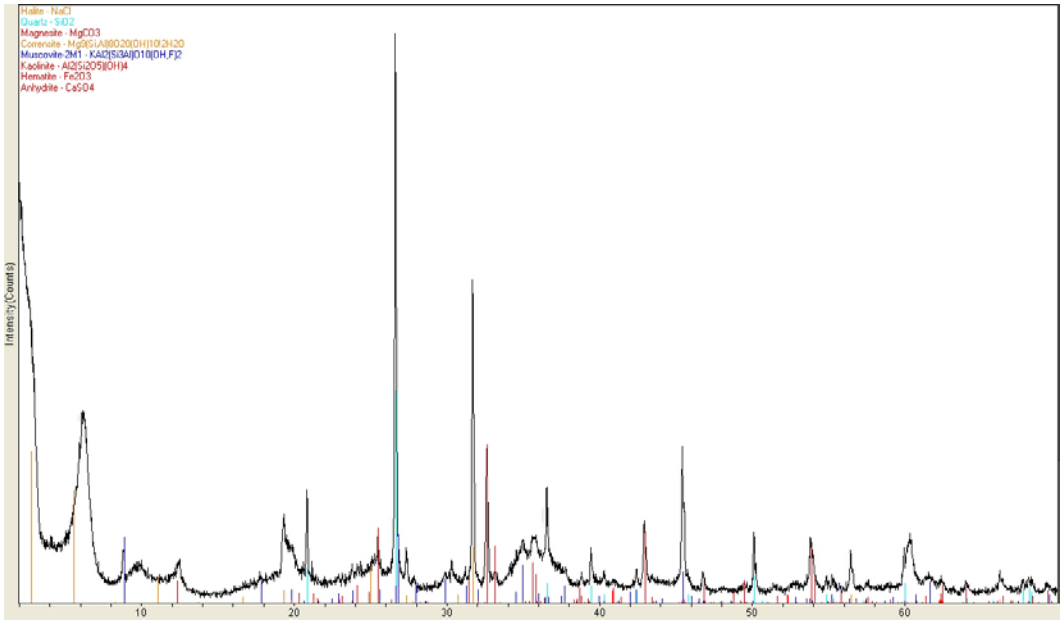

Figure 12. X-ray diffraction pattern of accessory minerals residues recovered by dissolving salt from clay seam F samples heated up to 265 ^{o}C.

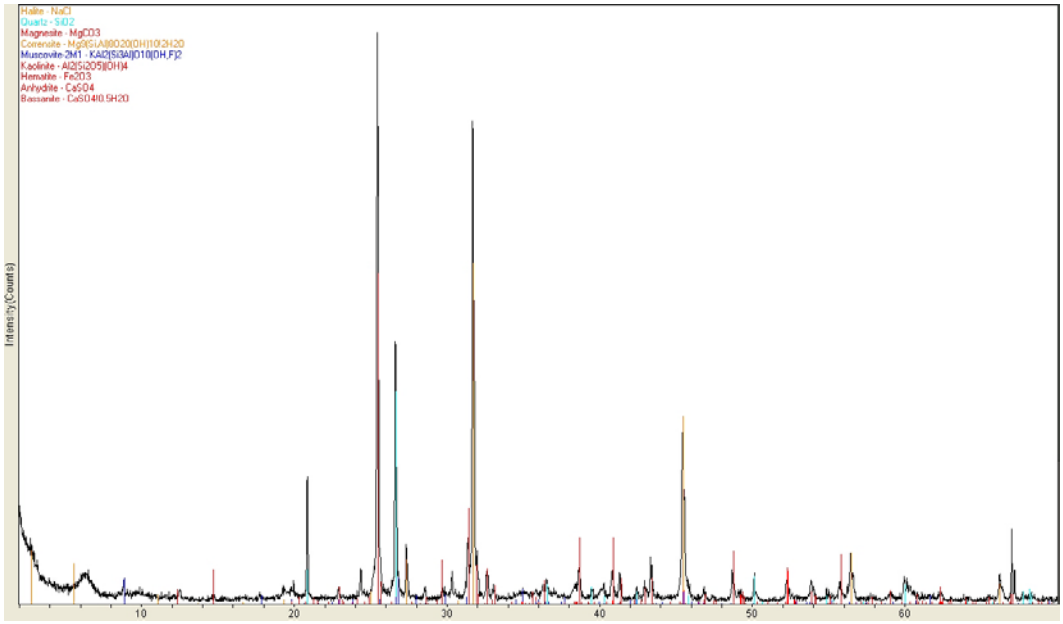

Figure 13. X-ray diffraction pattern of accessory mineral residues recovered by dissolving salt samples from the orange marker bed (heated to 265 ^{o}C).

3.1.2 Characterization of the porosity of crushed salt

The plot of the volume of brine added as function of volume increase in the crushed salt is shown in figure 14. The salt porosity was determined as the slope of the plot, which represents the volume of liquid, added over the volume increase

$$\Phi = \frac{V_V}{V_T}$$

Where V_v is the volume of the void space in the crushed salt and V_T is the volume of the bulk volume of the salt.

$\Phi = 0.39 \pm 0.02$

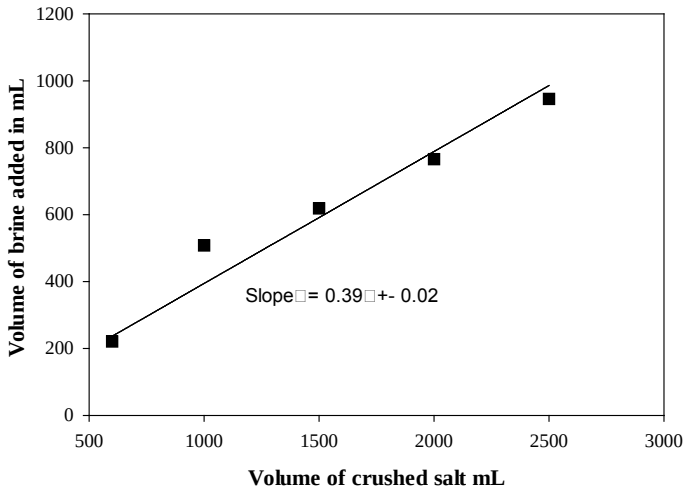

Figure 14. Plot showing the ratio of the volume of void space in crushed rock salt as a function of crushed salt volume used to determine crushed salt porosity.

3.1.3 Characterization of temperature profile in crushed salt intact small salt aggregates and intact salt core

We performed measurements to examine the temperature gradients is rock salt and crushed salt. The experiments were performed by heating the salt samples at one end using a heater cartridge and measuring the temperature in the salt as a function of the distance away from the heater. For crushed salt measurements, they were performed in a large beaker filled with crushed salt. The container was

instrumented with a heater cartridge controlled by a temperature controller and a series of thermocouples set at increasing distances from the heat source. The heat source temperature was fixed at 250 ^{o}C. The temperature of salt reached a steady state within hours but was left to equilibrate for 24 hours before the temperature measurements were recorded. The data in figure 15 show the temperature profile in crushed salt as a function of the distance from the heat source.

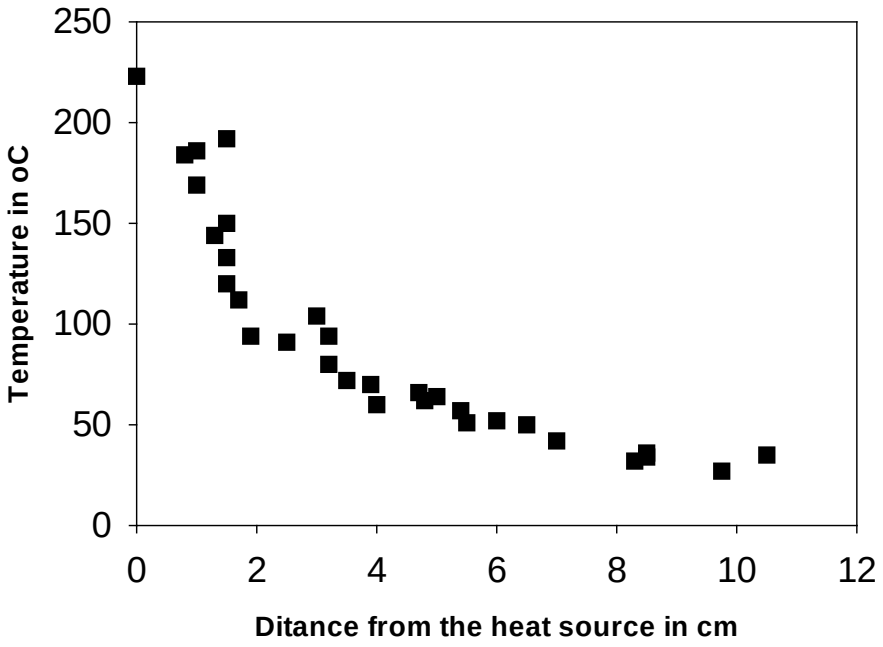

Figure 15. Plot showing measured temperatures in crushed salt heated using a 250 W heater cartridge. The temperature of the heater varied from 220 to 250 ^{o}C and the temperature was recorded using thermocouples 24 hours after the heating was started.

Large temperature gradients are rapidly established across the salt. The data show that there is lack of strong coupling between the heat source and salt. A significant temperature drop of 20 to 50 ^{o}C is observed in the immediate vicinity of the heat source. Temperature measurements near the heat source were affected by the heater radiating heat and were not very accurate (Figure 15). The temperatures decreased very rapidly as the distance increased away from the heat source. The temperature profiles

established rapidly following the initial heating (hours) and remained unchanged over time (observed for one week).

Large temperature gradients were also observed across salt crystals and salt aggregates heated on one side. We examined temperature gradients in salt aggregates by subjecting the salt crystals to a point heat source and monitoring temperatures as a function of the distance from the heat source. The data of the temperature profiles in a salt crystal subjected to a point heat source with surface temperature of 40, 80, 100, and 200 ^{o}C are shown in Figure 16. The data show that there is incomplete coupling between the salt and the heating block. The temperature of the salt in contact with the heating block is 5 to 20 ^{o}C lower than the temperature of the heating source. The temperature drop is more important at higher temperatures (Figure 16).

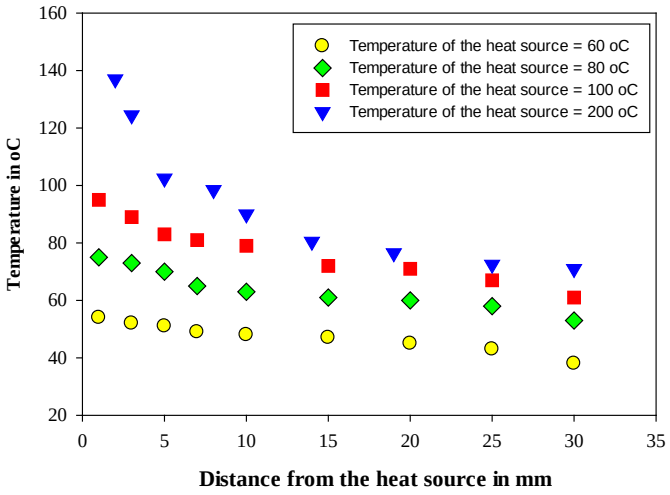

Figure 16. Plot showing the profile of temperature in intact small salt crystals established by point heating one surface of the salt crystal to 60, 80, 100, and 200 ^{o}C. The temperature reaches a steady state within about 10 min and remains stable (observed for up to 2 months). The temperature of the heat source was controlled buy a temperature controller that maintained the temperature with ± 1 ^{o}C from the desired temperature.

The data in figure 16 show the same rapid drop in the temperature away from the heat source and a low coupling between the temperature of the heating surface and the salt.

The crushed and intact salt experiments were modeled using LANL's Finite Element Heat and Mass transfer code (FEHM), which solves the governing equations of mass, energy, and momentum conservation for multiphase flow in porous media. New material models for the thermal properties of crushed and intact salt in FEHM are currently being developed and tested (Stauffer et al., 2012).

The intact salt crystal was modeled on a grid with 0.5 mm grid spacing in the crystal and 2 cm spacing in the surrounding air. The crystal was assumed dry. Within the salt crystal, thermal conductivity varies with temperature following:

$$\lambda = 5.4\left(\frac{300}{T}\right)^{1.14},$$

Where λ is thermal conductivity in $Wm^{-1}K^{-1}$ and T is temperature in K. The effective thermal conductivity of air in the model has a strong influence on the surface temperatures of the crystal. Estimates of effective air thermal conductivity for this system ranged from 0.5 to 1.0 $Wm^{-1}K^{-1}$ for combined conductive, convective, and radiative heat transfer in air. The best matches to the intact salt crystal data ranged from 0.25 to 0.4 $Wm^{-1}K^{-1}$, depending on the temperature of the heater. Figure 17 shows the experimental data and FEHM model results for the intact salt crystal at three temperatures (60, 80, and 100^{o}C) after 24 hours.

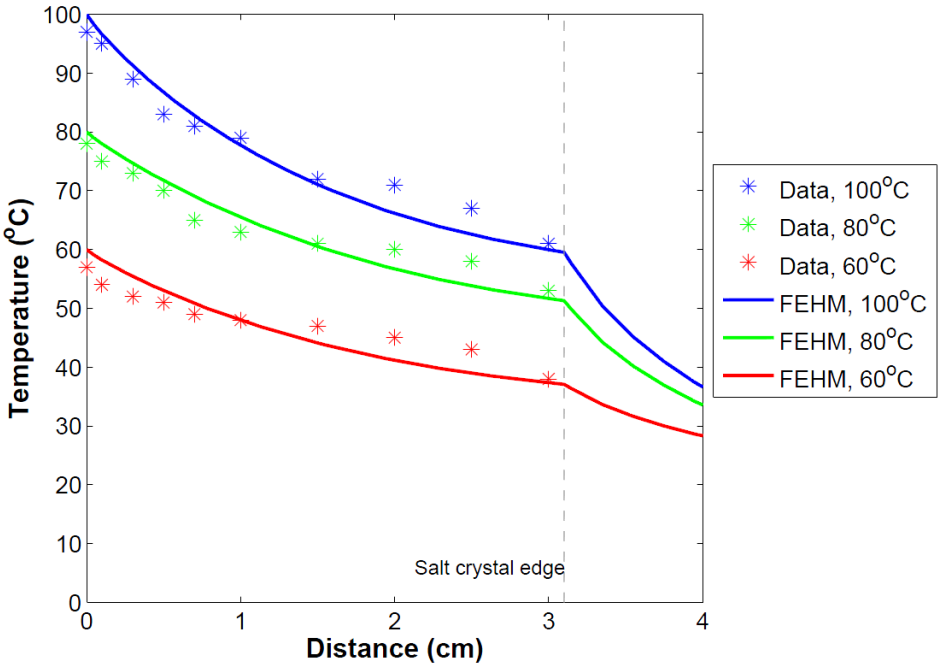

Figure 17. Intact salt crystal model results at 24 hours.

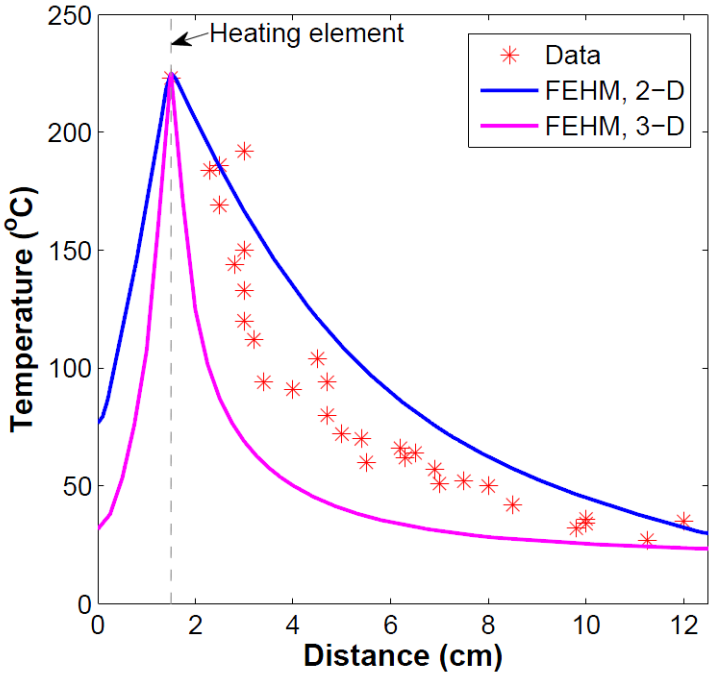

Figure 18. Crushed salt model results at 24 hours.

The beaker of crushed salt was modeled in 2-D and 3-D (Figure 18). The thermal conductivity function for crushed salt is both temperature- and porosity-dependent, and is given in Stauffer et al. (2012). The 2-D case stays warmer to greater distances than the experimental data due to the heating element having planar geometry in the 2-D model. In 3-D, the heating element was a line of nodes 1.5 cm from the edge of the beaker. As expected, the salt cools much more rapidly than in the 2-D case, but the temperature drop with distance is steeper than the experimental data. Additional investigations will be needed to analyze the model/data discrepancy.

3.1.4 Characterization of accessory minerals associated with white salt, red salt, clay seam F and orange maker bed

Accessory minerals from "clear" white salt, the red salt (Figure 19), and orange marker bed salt (Figure 20), orange marker bed salt (Figure 20), and clay seam F (Figure 21) were examined by XRD. All salt samples are dominated by halite (NaCl). The minor / accessory minerals are reported in Table 3. Corrensite, quartz, magnesite, muscovite and hematite are common to the units sampled. Anhydrite is present in all units except the red salt. Calcite and microcline are present only in the white salt; kaolinite is present in the orange marker bed, red salt and clay seam F, while bassanite is present in the white salt and orange marker bed.

Table 3. Minor / accessory minerals in Salado Formation (at WIPP) salt beds. All sedimentary beds contain the following common minerals (Corrensite, quartz, magnesite muscovite, hematite), while anhydrite is found in three of the sections sampled, and bassanite in two units.

White Salt	**Orange Marker**	**Red Salt**	**Clay Seam F**
Corrensite-$(Mg,Al)_9(Si,Al)_8O_{20}(OH)_{10}*4H_2O$	Corrensite-$(Mg,Al)_9(Si,Al)_8O_{20}(OH)_{10}*4H_2O$	Corrensite-$(Mg,Al)_9(Si,Al)_8O_{20}(OH)_{10}*4H_2O$	Corrensite-$(Mg,Al)_9(Si,Al)_8O_{20}(OH)_{10}*4H_2O$
Quartz-SiO_2	Quartz-SiO_2	Quartz-SiO_2	Quartz-SiO_2
Magnesite-$MgCO_3$	Magnesite-$MgCO_3$	Magnesite-$MgCO_3$	Magnesite-$MgCO_3$

Muscovite- $KAl_2(Si_3Al)O_{10}(OH)_2$	Muscovite- $KAl_2(Si_3Al)O_{10}(OH)_2$	Muscovite- $KAl_2(Si_3Al)O_{10}(OH)_2$	Muscovite- $KAl_2(Si_3Al)O_{10}(OH)_2$
Hematite-Fe_2O_3	Hematite-Fe_2O_3	Hematite-Fe_2O_3	Hematite-Fe_2O_3
Anhydrite-$CaSO_4$	Anhydrite-$CaSO_4$		Anhydrite-$CaSO_4$
Bassanite- $CaSO_4*0.5H_2O$	Bassanite- $CaSO_4*0.5H_2O$		
Calcite-$CaCO_3$			
Microcline-$KAlSi_3O_8$	Kaolinite- $Al_2(Si_2O_5)(OH)_4$	Kaolinite- $Al_2(Si_2O_5)(OH)_4$	Kaolinite- $Al_2(Si_2O_5)(OH)_4$

The following XRD patterns verify the mineral assemblages collected at the repository horizon. Figure 19 presents minerals identified in the red salt bed, Figure 20 the orange marker bed, and Figure 21 the clay seam F.

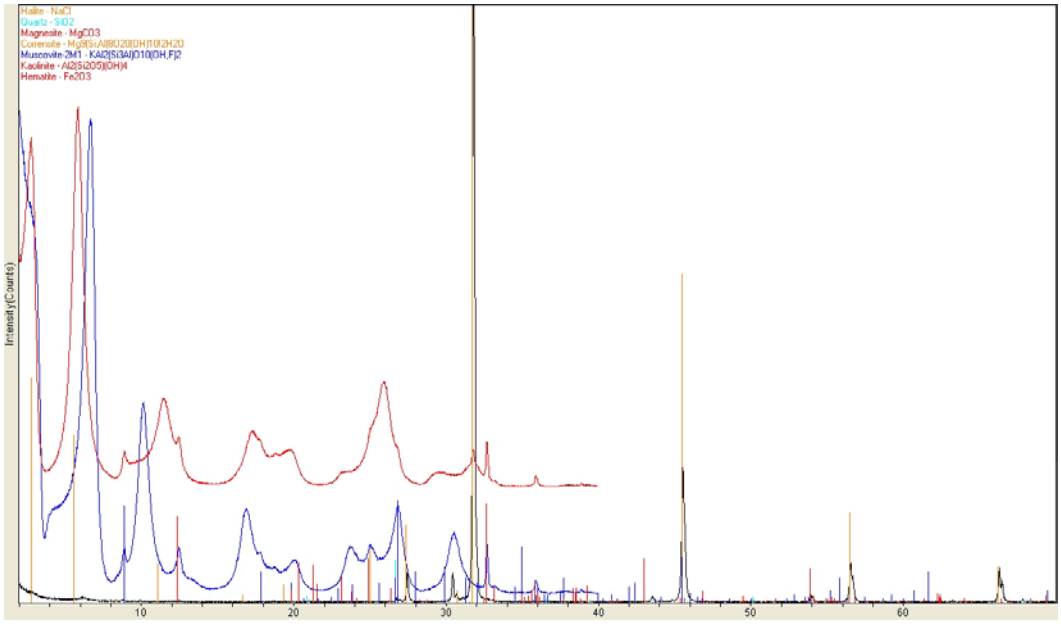

Figure 19. Minerals identified in the red salt bed. Red and blue spectra are kaolinite and muscovite standards.

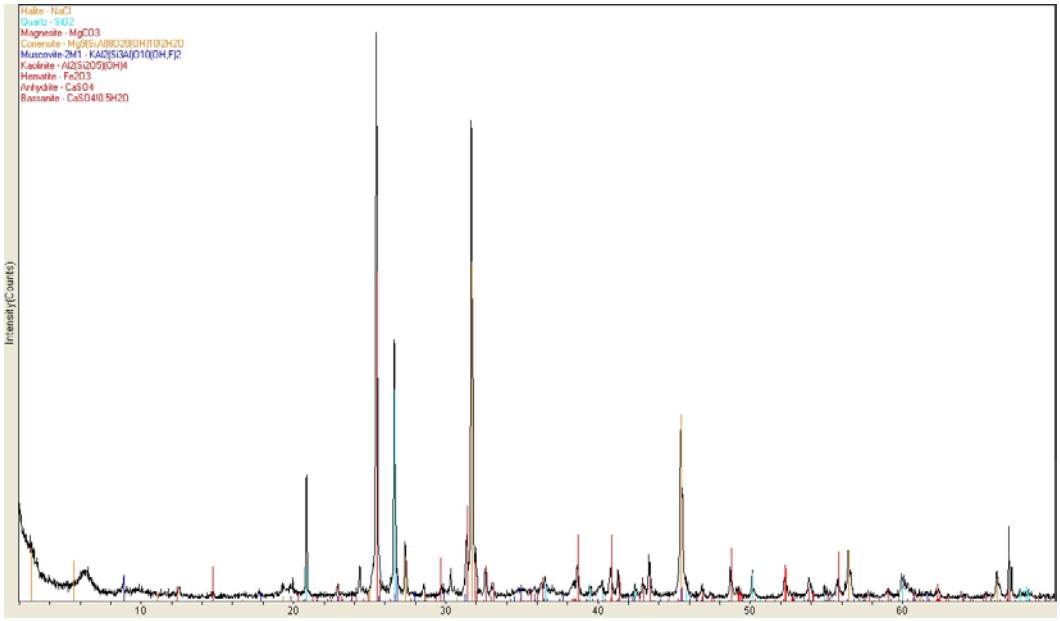

Figure 20. Accessory minerals of the orange marker bed.

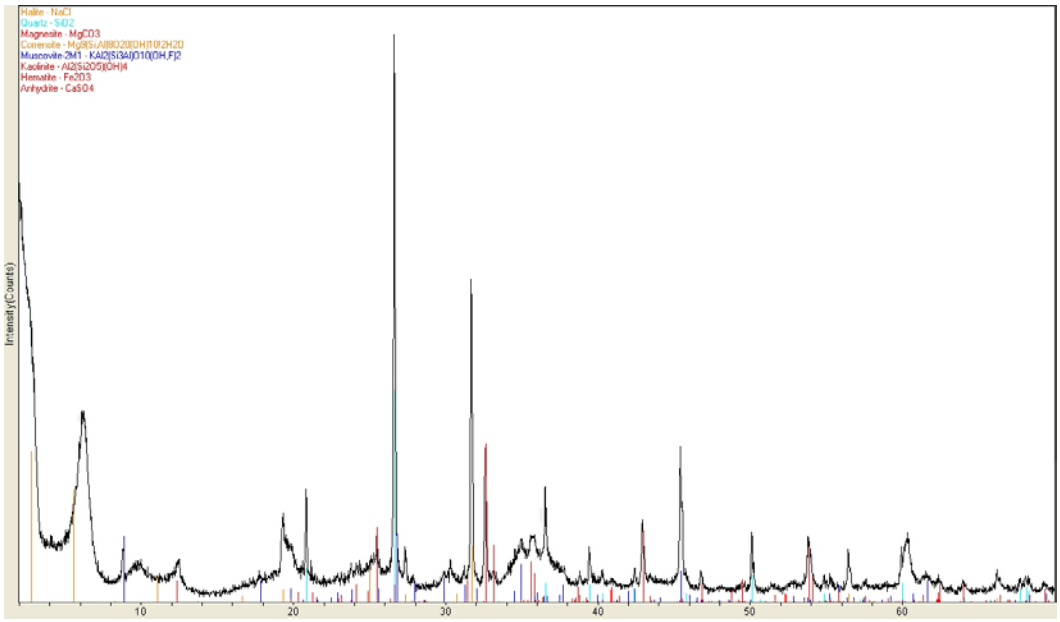

Figure 21. Minerals identified in Clay seam F.

3.2 Laboratory examinations of clay and gypsum dehydration as a function of temperature

3.2.1 Corrensite dehydration results

Corrensite has been documented previously by Krumhansl et.al. (1990) at WIPP. The corrensite clay dehydration examinations were performed using in situ XRD characterization performed with an environmental cell connected to a humidity generator which allows for XRD measurements to be performed under controlled conditions of RH and temperature (RH-XRD). The data presented show that corrensite dehydration occurs at < 100 ^{o}C (Figure 22). This is indicated by the multiple peak shifts from the 25 ^{o}C to the 100 ^{o}C run, with the prime example being the d_{002} reflection peak shift from 13.3 to 12.1 Å. The experiments at 300 ^{o}C, 150 bar indicated no further water release occurred. It was important to narrow down the temperature at which the dehydration transition occurred, so further heated stage XRD runs were performed. Figure 23 shows Corrensite heated stage XRD runs from 25 ^{o}C to 100 ^{o}C at approximately 10 ^{o}C intervals with an RH of 30 – 35%. Note that there are two peak shifts, 13.7 to 12.3 Å and 9.1 to 8.6 Å, respectively over the 75 ^{o}C experiment range. These results allowed for a final experiment (Figure 24) that centered on collecting Corrensite diffraction patterns at 65 and 75 ^{o}C. The diffraction patterns in Figure 24 indicate that there is a significant loss of interlayer water in the corrensite structure between 65 and 75 ^{o}C, as indicated by the peak shifts at 13.0 to 12.6 Å and 8.64 to 8.22 Å, respectively. By mapping the (001) d-spacing to temperature (Figure 25) one can see that there is a significant and abrupt water loss between 65 and 75 ^{o}C. The site of interlayer water molecules in corrensite is depicted in Figure 26. The chemical description of this dehydration is as follows:

$$(Ca, Na, K)(Mg,Fe,Al)_9(Si,Al)_8O_{20}(OH)_{10}9H_2O = (Ca,Na,K)(Mg,Fe,Al)_9(Si,Al)_8O_{20}(OH)_{10} + 9\ H_2O$$

This interlayer water dehydration from stoichiometric corrensite would release 13 wt% water.

Lippmann (1976) presents a model of corrensite swelling where a fully dehydrated corrensite (above 200 ^{o}C) has a unit cell of 24 Å, the clay with interlayer water has a unit cell of 29 Å, and a fully saturated (i.e. moist) corrensite crystal has a unit cell of 33 Å. The author also indicates that the clay can hydrate – dehydrate reversibly and completely. It is this action that he attributes to the cause of floor heaves in tunnels in the Keuper Formation in Germany. Based on thermodynamic modeling, Vidale and Dubacq (2009) describe a similar hysteresis for smectites. The hydration – dehydration reversibly described holds true until there is a phase change at higher temperatures. Velde (1977) constructed phase diagrams using experimental data to constrain the stability of illite-montmorillonite, corrensite, expanding chlorite, and illite. The author states that the Me^{3+} (i.e. Al^{3+} and/or Fe^{3+}) content of the assemblage, along with temperature and pressure constraints, will control whether an expanding chlorite or corrensite will appear. Using the diagrams produced by Velde (1977) corrensite, as sampled from WIPP, would have a large phase stability field under generic proposed repository conditions. Ryan and Hillier (2002) describe the co-existance of 3 layered phyllosilicates (berthierine/chamosite, corrensite, and chlorite) in evaporite associated facies of the Sundance Formation in Wyoming. Although the formation is predominantly sandstone, the clay rich facies give some insights into the formation and stability of the corrensite present. The authors state that the corrensite forms authigenically from saponite during burial diagenesis. They also discussed various lines of evidence to imply that the diagenetic conditions did not exceed 4000 m depth and 120 ^{o}C.

All evidence discussed indicates that corrensite is stable under present day conditions in the Salado Formation. The samples we collected were fully saturated and were shown to lose the interlayer water between 65 and 75 ^{o}C. From the discussion above, the corrensite clay should be able to rehydrate once temperatures drop below 65 ^{o}C. However two variables are presently unknown. First, will hydration occur in a clay rich bed under lithostatic pressure conditions after closure of a repository? Second, will there be free water available to rehydrate the clays? We believe these are important factors that deserve further research.

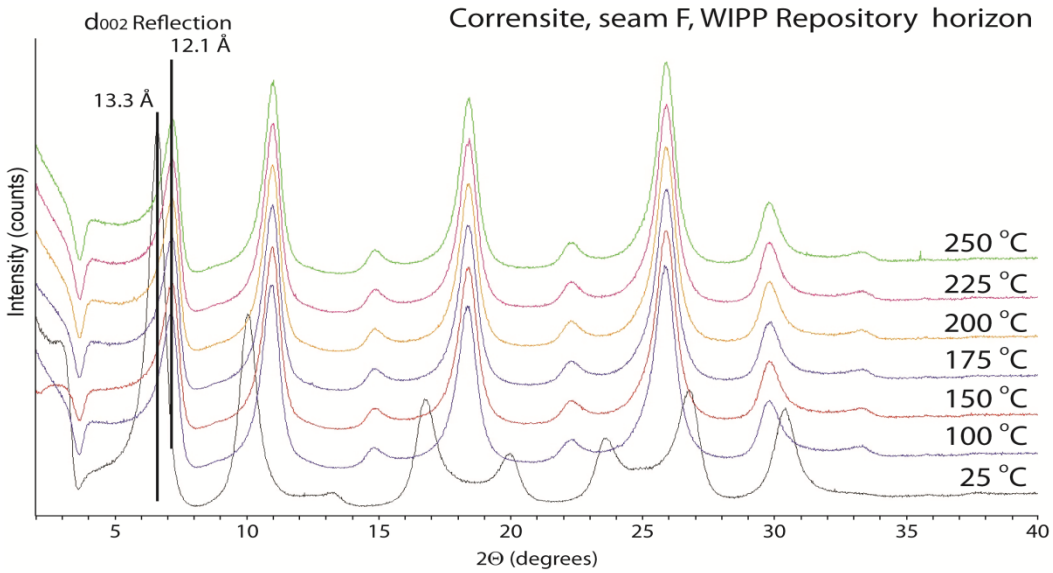

Figure 22. Corrensite thermal profile.

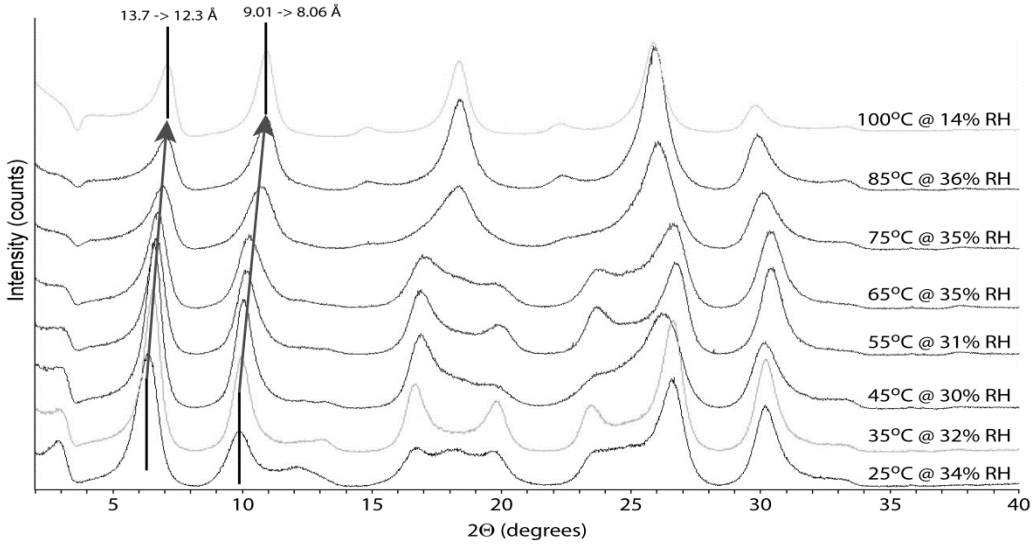

Figure 23. Corrensite 25 to 100 C.

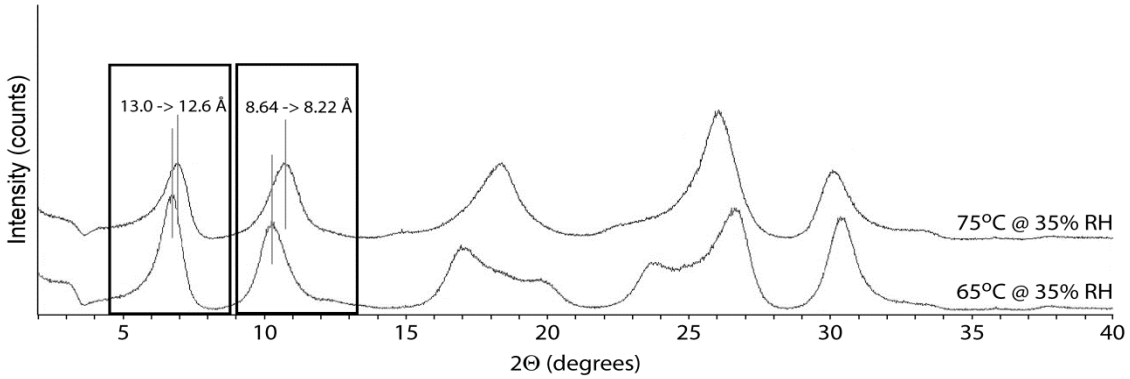

Figure 24. Corrensite 65- 75 C.

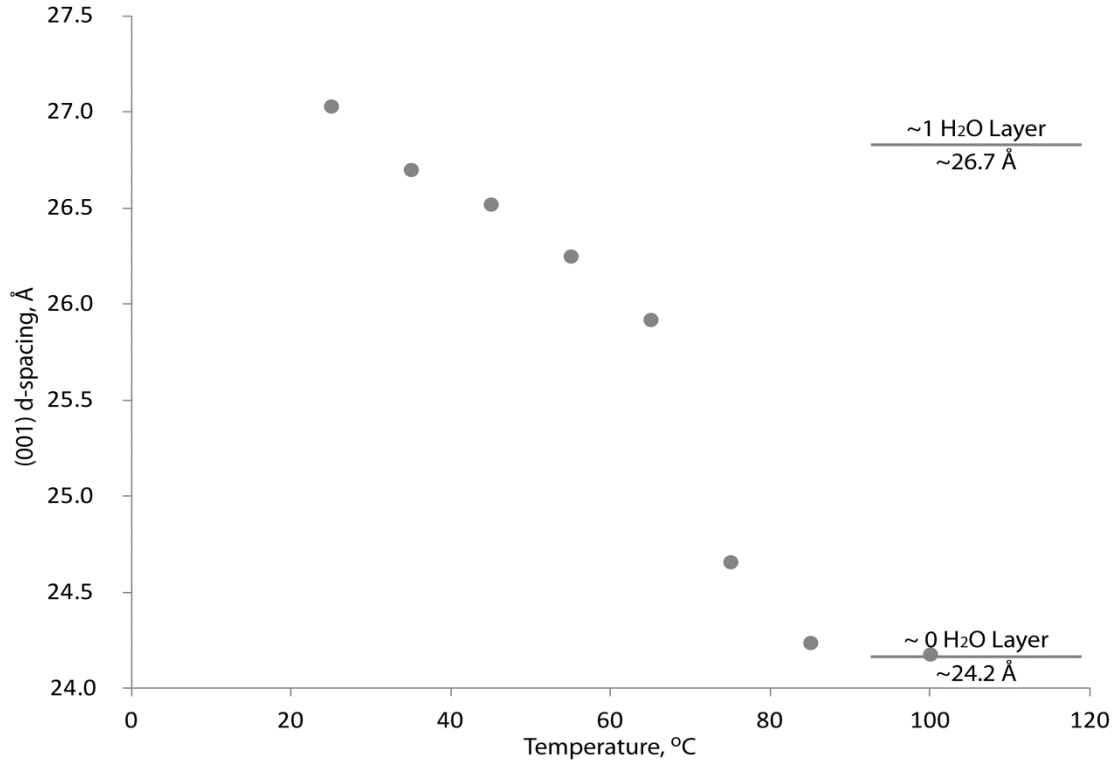

Figure 25. Corrensite dehydration as shown by (001) d-spacing reduction.

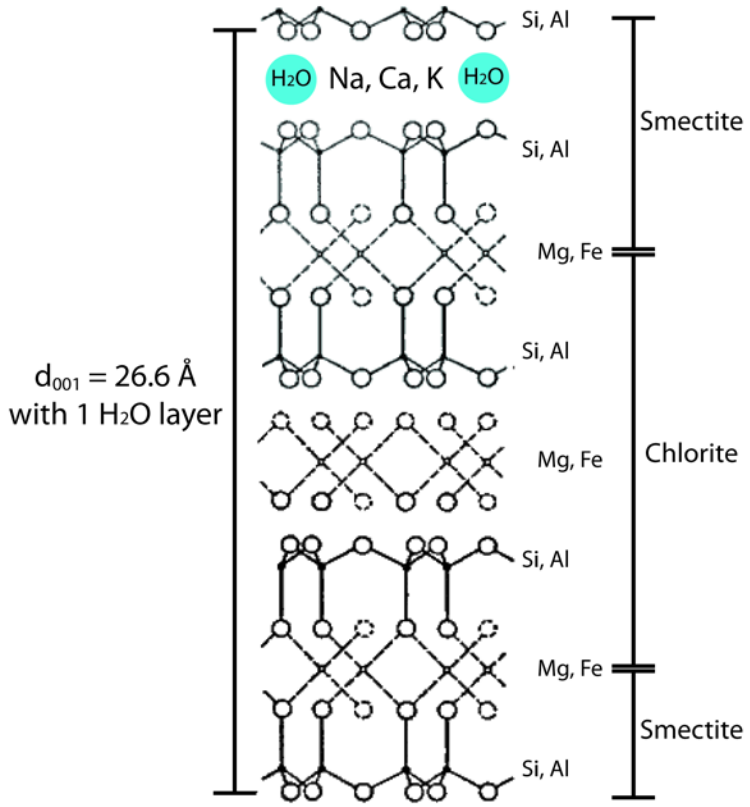

Figure 26. Corrensite structure. Loss of interlayer water molecule.

3.2.2 Sulfate dehydration

Determination of Salado Formation salt minor phases at WIPP by powder XRD indicate the presence of bassanite, anhydrite, and polyhalite (Table 3). A “polyhalite” bed examined by XRD reveals that in fact anhydrite exceeded polyhalite by three to one. Low overall sulfate abundances in the Salado Formation horizons of interest necessitated the use of gypsum samples from Naica Mexico (Figure 27) for the phase stability studies. There are two possible dehydration reaction pathways for gypsum: 1) gypsum to anhydrite, and 2) gypsum to bassanite to anhydrite. The chemical reactions are as follows:

One Stage

Gypsum = Anhydrite + water

$CaSO_4\ 2H_2O$ = $CaSO_4$ + $2H_2O$

Two Stage

Gypsum = Bassanite + water = Anhydrite + water

$CaSO_4\ 2H_2O$ = $CaSO_4\ 0.5H_2O$ + 1.5 H2O = $CaSO_4$ + $0.5H_2O$

Either dehydration reaction series creates a large water release (21% wt. loss) and volume reduction (~40%). Such a large water loss from the crystal structures and resulting volume contraction may induce fractures in the evaporite beds.

Using an environmental XRD cell connected to a humidity generator which allows for measurements to be performed under controlled conditions of RH and temperature, we captured the first phase transition from gypsum to anhydrite (using the gypsum sample from Naica, Mexico), which reveals that bassanite forms at approximately 75 ^{o}C, 1 bar (Figure 27). As shown in Figure 27, when gypsum is analyzed with the XRD, there is an abrupt phase change at 75 ^{o}C to bassanite. At this temperature, there is some remnant gypsum identified, but is most probably due to kinetic effects. In recent work bassanite is present from 75 to 275 ^{o}C, 1 bar, as shown in Figure 28. Figure 28 represents a time series of XRD spectra for bassanite after Naica gypsum was heated to 275 ^{o}C. Note that there is a slow in-growth of anhydrite and that the anhydrite abundance increases with time. Bassanite phase stability at higher temperatures is not yet determined, but experiments are ongoing.

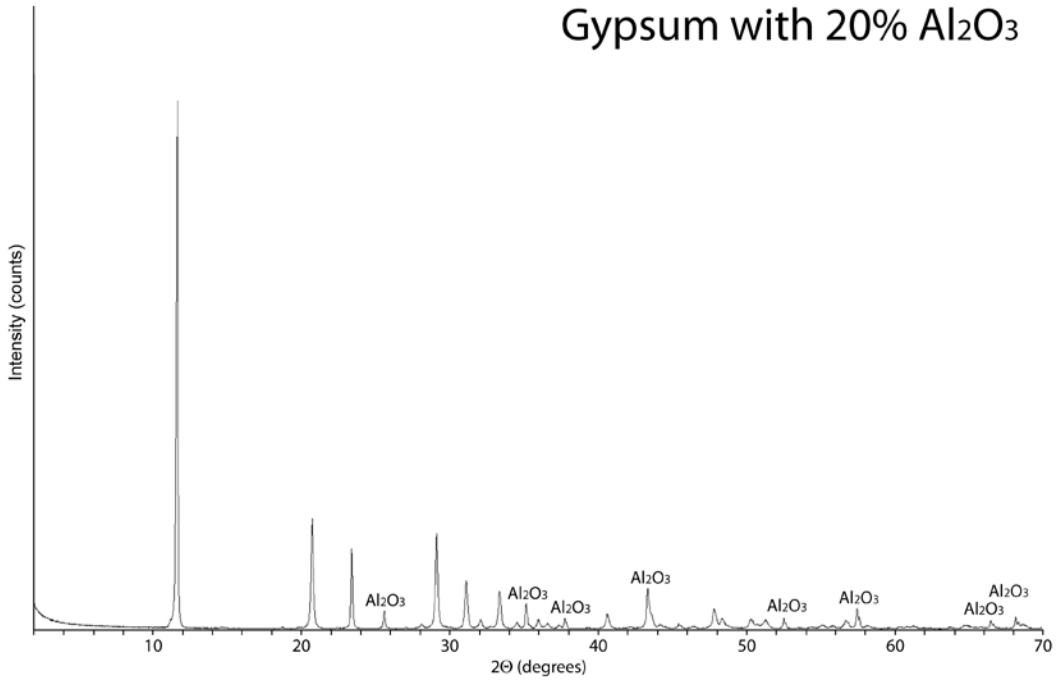

Figure 27. X-ray diffraction pattern of Gypsum samples from Naica Mexico used in our experiments. Temperature = 25 ^{o}C, RH = 14 %.The sample was ground and mixed with 20% corundum (Al_2O_3) used as a reference material for quantitative analysis.

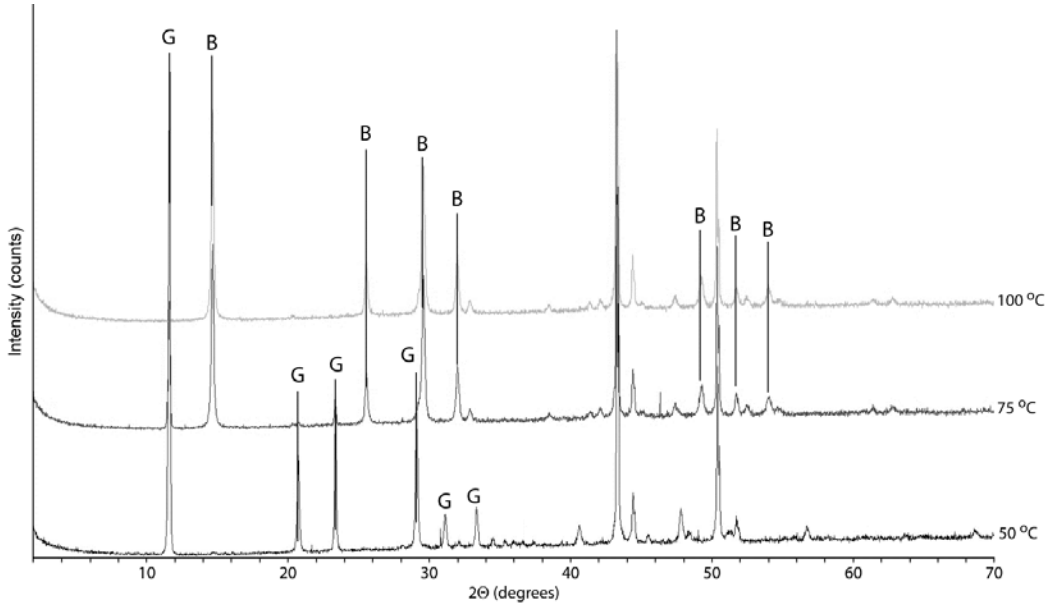

Figure 28. X-ray diffraction patterns showing the Gypsum to Bassanite transformation in situ by heating Naica gypsum samples at 50, 75, and– 100 ^{o}C. The relative humidity was 14%.

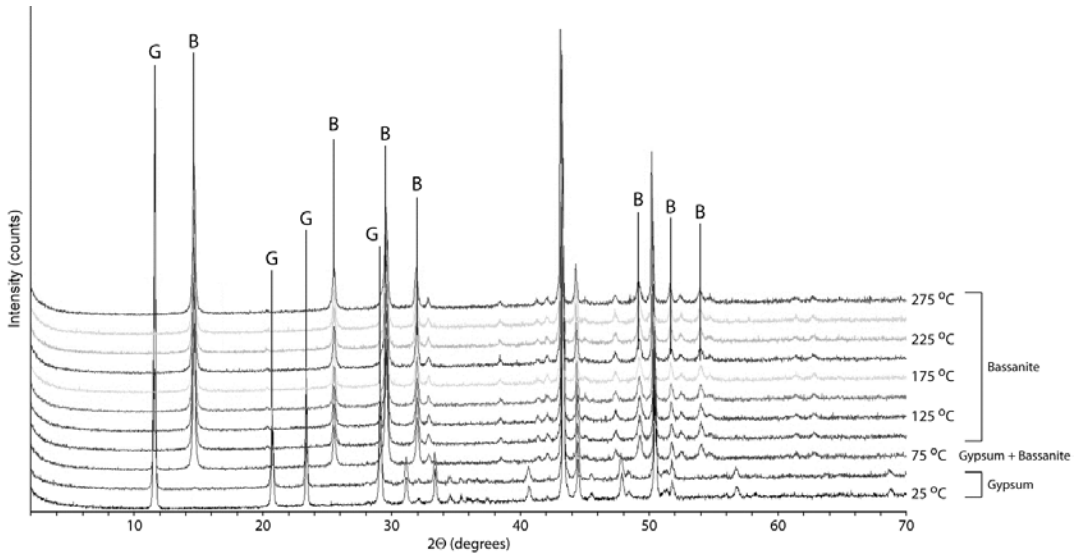

Figure 29. X-ray diffraction patterns show the Gypsum to Bassanite transformation as a function of temperature. RH varied between 31 to 34%.

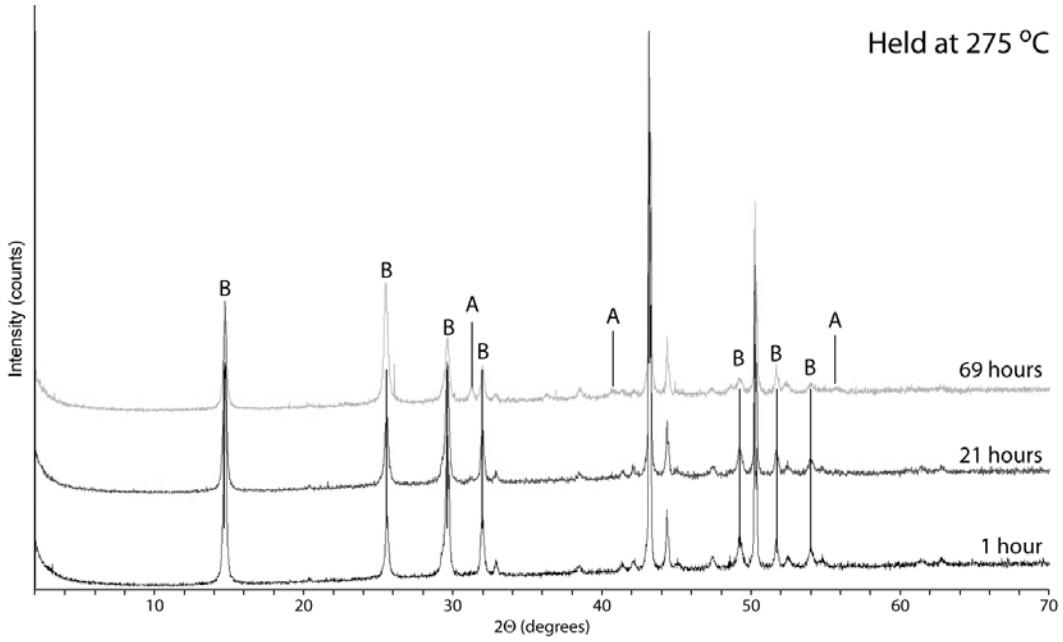

Figure 30. X-ray diffraction patterns of bassanite recorded over time at a constant temperature of 275 °C. The different spectra represent heating time of 1, 21, and 69 hours respectively. RH was maintained at 31 to 34 %.

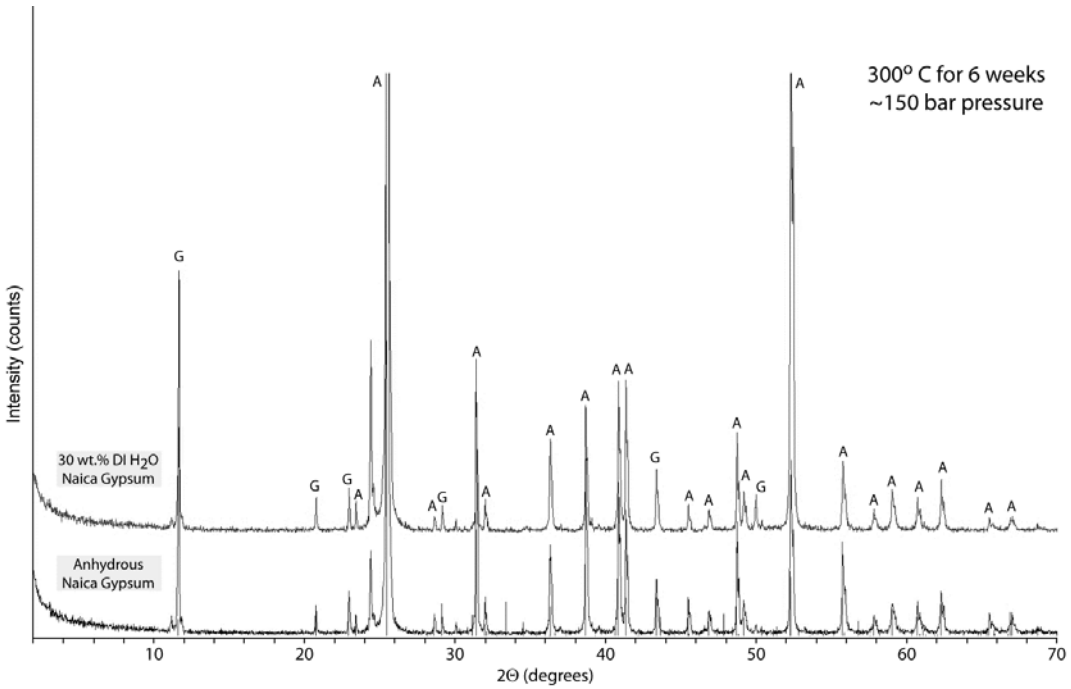

Figure 31. X-ray diffraction patterns showing gypsum to anhydrate transformation. Gypsum was held for 6 weeks at 300°C and 150 bars, proof of formation of anhydrite from gypsum. Note that remnant gypsum still occurs; indicating that kinetics of reaction is slow. Bassanite, which does not occur, is metastable under these conditions.

Figure 31 depicts the results of experiments run at 300 °C and 150 bar using gold capsules within our hydrothermal autoclaves. The XRD spectra show that anhydrite is stable, bassanite no longer occurs, and remnant gypsum is still present. These experiments were run both "dry" (i.e., gypsum powder starting material) and saturated with DI. The remnant gypsum is likely present due to the slow kinetic gypsum to anhydrate transformation.

Both type of experiments (1 bar and 150 bars, with various liquid water contents) indicate differing phase stabilities. Time, temperature and pressure all seem to be controlling factors affecting the stability of metastable bassanite (Shcherban and Shirokikh, 1971). The two step reaction involving a metastable phase results in researchers determining wide stability differences. Reasonable boundaries may be (1) gypsum to bassanite transformation at 76 °C (Freyer, 2000) and (2) bassanite to anhydrite at 100 to 140 °C (Shcherban and Shirokikh, 1971). Robertson and Bish (2013) set about looking at Ca-sulfate stability on

Mars, however their heated stage XRD experimental results, which covered a range of temperatures (below freezing to 200+ ^{o}C) and relative humidity RH ranging from 0 to 100% made the results pertinent to high temperature salt repositories. Their determination of the bassanite to anhydrite transformation occurred at temperatures as low as 85 ^{o}C at PH_2O of 1300 Pascals. This temperature climbed slightly as the PH_2O declined. The authors stated that bassanite is completely unstable at RH < 1.2%, and that gypsum rehydration from bassanite only occurs at 100 % RH. Robertson and Bish (2013) also conclude that the dehydration reactions are sluggish, due to kinetic factors. Determining the metastable bassanite field would be critical to understanding the water release timing and amounts in a high temperature repository setting.

3.2.3 Thermogravimetric Analysis (TGA) of salt samples from WIPP

Figure 32 shows TGA results obtained for rock salt (white) (sample 1), rock salt with clay (sample 2), and a leached rock salt/clay (sample 3).

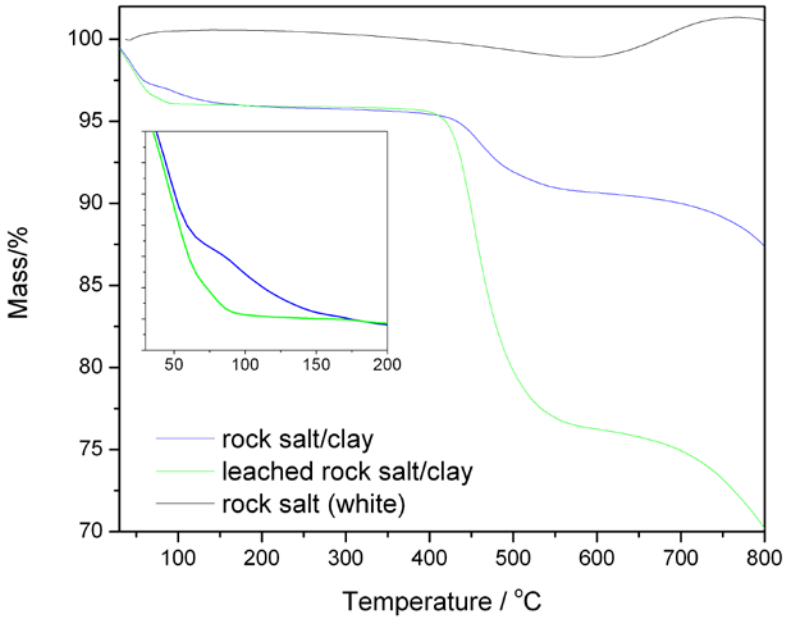

Figure 32. Combined TGA results for sample 1 (rock salt (white)), sample 2 (rock salt/clay), and sample 3 (leached rock salt/clay).

TGA results show no measurable weight loss from clear salt (sample 1) over the entire temperature domain examined (T up to 600 ^{o}C). The sample gained some weight at elevated temperatures > 600 ^{o}C. Sample 3 lost weight in two stages. The first weight loss which represents a mass loss of about 4% occurred from room temperature to ~ 75^{o}C and the second weight loss representing an additional mass loss of about 19 % occurred between 400 and 600 ^{o}C. This sample represents the insoluble mineral fraction obtained from sample 2. It consists primarily of corrensite and other minor accessory minerals associated with Salado Formation salt (Table 3). The results of the first weight loss are consistent with the results obtained during our corrensite dehydration studies and is attributed to the loss of interlayer water (figure 26). It is also consistent with the thermogravimetric studies which show mass losses of up to 3 wt% at 65 ^{o}C in clay rich samples (Table 2). The second weight loss at higher temperature is attributed to a phase change of clay to mica. However, no structural characterization was performed to determine the nature of the structural changes that occurred, as these transformations occur at much higher temperatures than is expected in repository setting.

Sample 2, which contains clear salt and the clay rich accessory minerals shows a slightly different weight loss profile. Three distinct weight loss stages can be distinguished. The first weight loss occurs at moderate temperature of < 75 ^{o}C and represents a water loss of about 2.8 wt %. This is consistent with the loss of interlayer water in corrensite clay. The magnitude of the weight loss is consistent with the water loss determined from the thermo gravimetric studies (table 2). The second weight loss with a magnitude of 1.4 wt% occurs at slightly higher temperatures of about < 200 ^{o}C. We don't have any direct characterization of the transformation responsible for the weight loss observed. However, given the mineralogical composition of the mineral residues present in Salado Formation salt, it is possible that this weight loss is due to gypsum to bassanite phase transformation characterized in our study. The last weight loss T > 400 ^{o}C is due to mineral transformations that occur at higher temperatures (i.e., sulfate and chloride minerals decomposition), but have not been investigated in this study. The difference in weight loss between sample 2 and sample 3 is likely due to a difference in their total clay content which we have

documented in the thermogravimetric study (Figure 11) to determine the magnitude of the samples weight loss.

Detailed information on TGA of three samples is presented in Figures A.1, A.2, and A.3 in appendix A. The figures show detailed analysis of the weight percent loss of water, which is marked in each individual figure. These data are consistent with the water loss and phase changes observed in the in situ characterization of clay and sulfate dehydration by XRD presented in the previous section.

3.2.4 Characterization of water associated with salt using Filter Difference Spectrometry (FDS)

The most striking aspect of FDS spectroscopy is the number of discernible peaks available for interpretation in the spectrum. Whereas in infrared spectroscopy, three normal modes are observed for water with barely interpretable and discernible shifts, FDS shows a plethora of modes each attributable to a different vibrational state associated with a specific state of water. In this section we will only discuss the behavior of the principal peak at ~700 cm^{-1} wavenumbers. This peak is assigned to the presence of free water (i.e. water which fluid inclusions). Figure 33 depicts a FDS raw spectrum of sample 2 which is rock salt rich is clay.

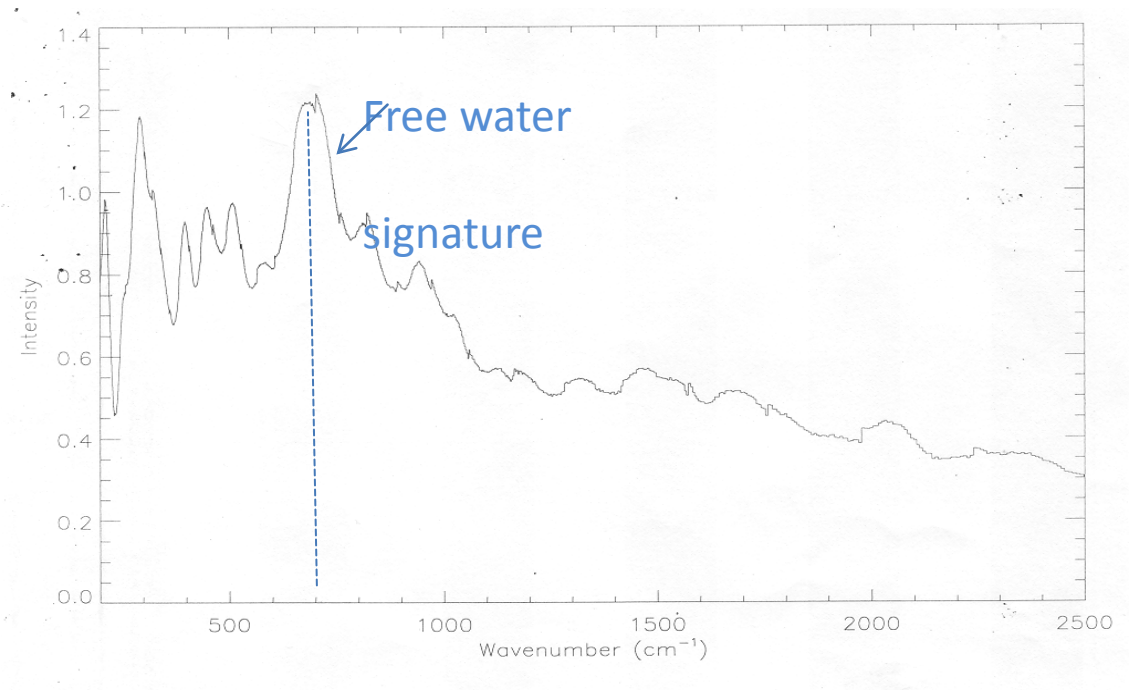

Figure 33. Raw FDS spectrum of (rock salt with clay) sample 2. Inclusion water in salt is clearly seen at ~ 700 wavenumber cm^{-1}.

Besides fluid inclusions, water can also be structurally incorporated in hydrous minerals in rock salt. The water associated with clays and/or other minerals is crystallographically bound and shows different vibration states of water, as shown in Figure 34. A combined FDS result of sample 2 and 3 is presented in Figure 35. As can be seen from Figure 35, sample 3 has no free water (fluid inclusions) as observed from the lack of the free water signature peak at ~ 700 wavenumber (cm^{-1}), and is significantly different from the mixed clay / salt sample (sample 2) containing fluid inclusions. For sample 3, this particular peak almost disappeared due to lack of salt fluid inclusions in the sample. Figure 35 also shows rich vibration states of hydrogen bond associated with clays and sulfates, as indicated by many sharp peaks and spectra.

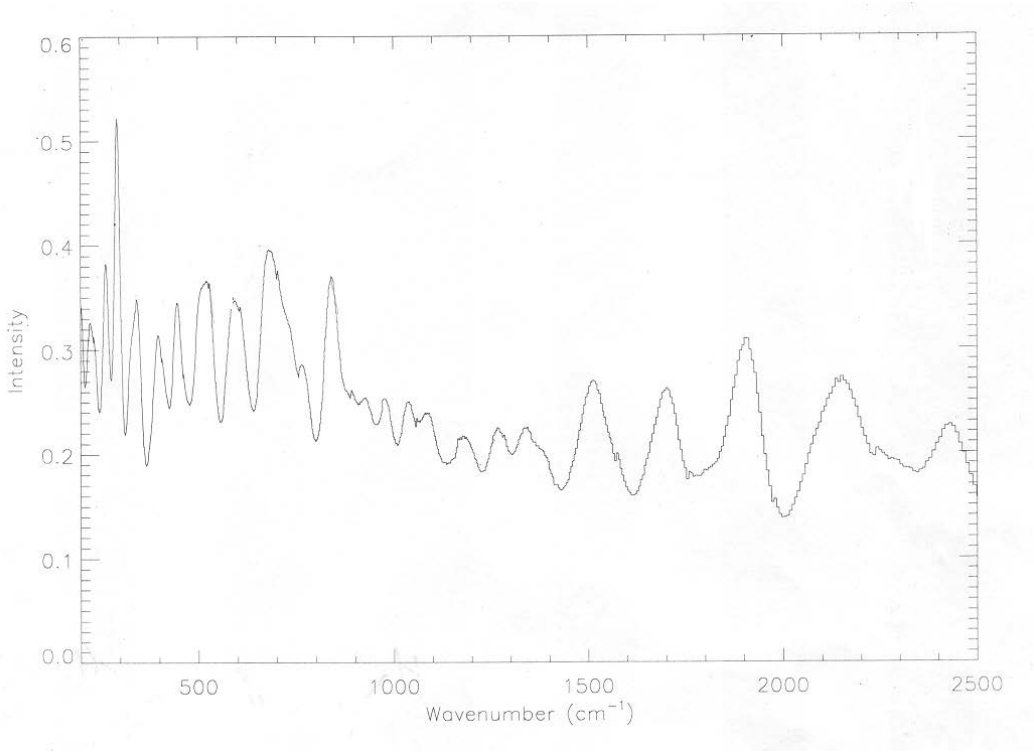

Figure 34. Raw FDS spectrum of residual clay and other accessory minerals sample 3.

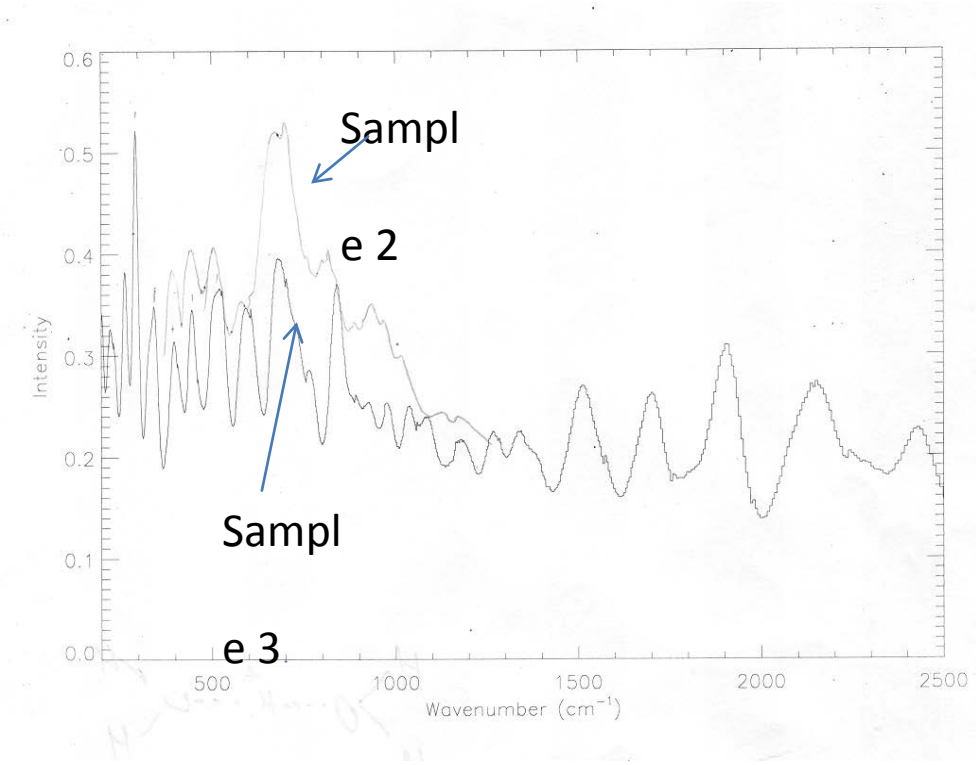

Figure 35. Combined raw FDS spectra of (rock salt with clay) sample 2 and residual clay and other accessory sample 3.

The characterization of different type of water in salt (e.g., bulk water in the forms of fluid inclusions, surface water present as grain-boundary fluids, and water bound within secondary minerals, e.g., clay and sulfates), and their mobility and evolution as a function of temperature are pertinent factors needed for salt repository modeling.

This preliminary study suggests that neutron based Filter Difference Spectrometer (FDS) holds promise as a viable technique offering an insight to the nature of waters in salt. It is well suited to fingerprint different types of water in geological materials (e.g., structural water, bulk water, and surface water at a larger scale due to the size of the sample chamber).

By combining TGA with mineral dehydration studies, FDS may show promise for scaled up experiments to characterize and quantify water content in salt at a larger scale (core size or greater). Thus, further investigations in multi-staged phases and scales should be conducted.

3.3 Laboratory examinations of brine inclusion migration in a thermal gradient.

Measurements were performed on single salt crystals containing brine inclusions, which varied in size from sub millimeter to millimeters. Typical experiments consisted of heating single salt crystals on one side using a point heat source mounted on a microscopy heating stage and recording still images of the salt crystals. Analysis of the still images allows determination of the morphology of the individual inclusions in salt and their migration over time due to a heat source. The rates of the inclusion migration were determined by analyzing the distance traveled by the inclusions as a function of the inclusions distance from the heat source. The surfaces of the salt crystals used in the examinations were polished using a paper towel wetted with DI water to enhance the transparency of the salt and improve the visualization. The temperature gradients applied during the experiments were determined by the

temperature of the heated block. Temperatures of 200, 150, 100, and 60 ^{o}C were used in various experiments. The temperatures decreased rapidly and exponentially away from the heat source and thermal gradients were established rapidly (~ 15 min) and remained stable for the entire experiment. At the completion of the heating experiment the salt crystals were sectioned along the inclusions migration pathways and mounted for analyses by SEM-EDS. All images were processed using Photoshop and VirtualDub.

3.3.1 Single phase inclusion migration in a thermal gradient

The salt crystals selected for the examination of liquid phase inclusion in a thermal gradient contained inclusions of variable sizes and distances from the heat source. The behavior of the inclusions after the start of the heating experiment was dependent on the heat load, the size of the inclusion, and the inclusions position within the salt crystal. Large inclusions (~ mm size) that are near the surface usually don't migrate far from their original location and tend to burst to the surface when the pressure buildup is sufficient to break the salt. This process results in a flash water evaporation and the deposition of a cone shaped salt efflorescence at the surface of the salt crystal. The series of photographic pictures shown in Figure 36 show images of a salt crystal heated to 200 ^{o}C at one end and left to establish a natural gradient along the salt length. The successive images illustrate the evolution of the brine inclusion as a function of time.

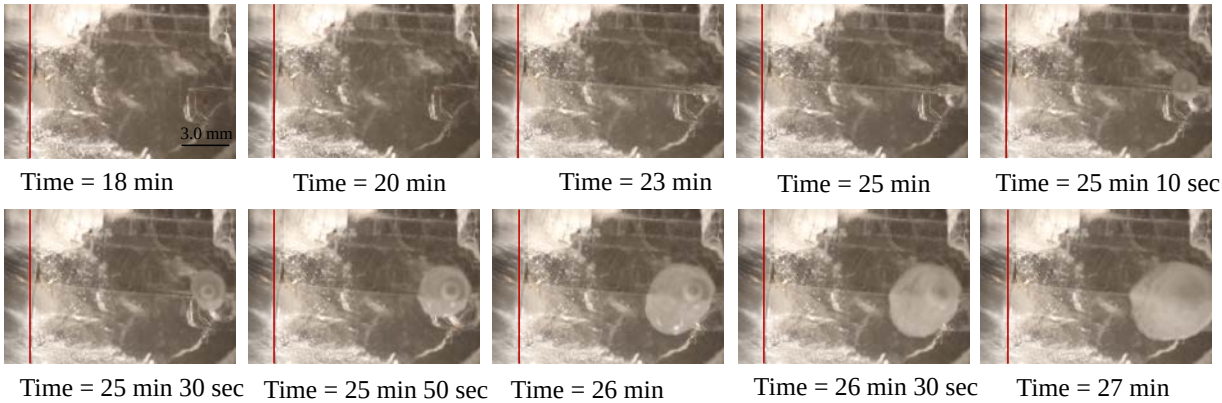

Figure 36. Still images showing the evolution of a brine inclusion close to the surface as function of time. Temperature at the heat source (marked with a red line) was fixed to 200 ^{o}C.

The images show that at high temperatures and inclusions are near the surface, the heat results in the creation of small vapor bubbles within the inclusion that coalesce to form a larger bubble (time 18 to 25 min). The creation of a vapor phase results in the over pressurization of the inclusions and fracture of the salt (visible at time 23 min on the figure). The brine then escapes rapidly through the facture and evaporates rapidly leaving a cone shaped salt deposit.

Full brine inclusions that are not sufficiently large or that don't get heated sufficiently to fracture the salt crystal migrate slowly towards the heat source (up the temperature gradient). The migration processes undergoes three distinct stages. The first stage consists of a transition state in which the inclusions change shape. Figure 37 shows a time series of still images collected during the initial stage of inclusions migration.

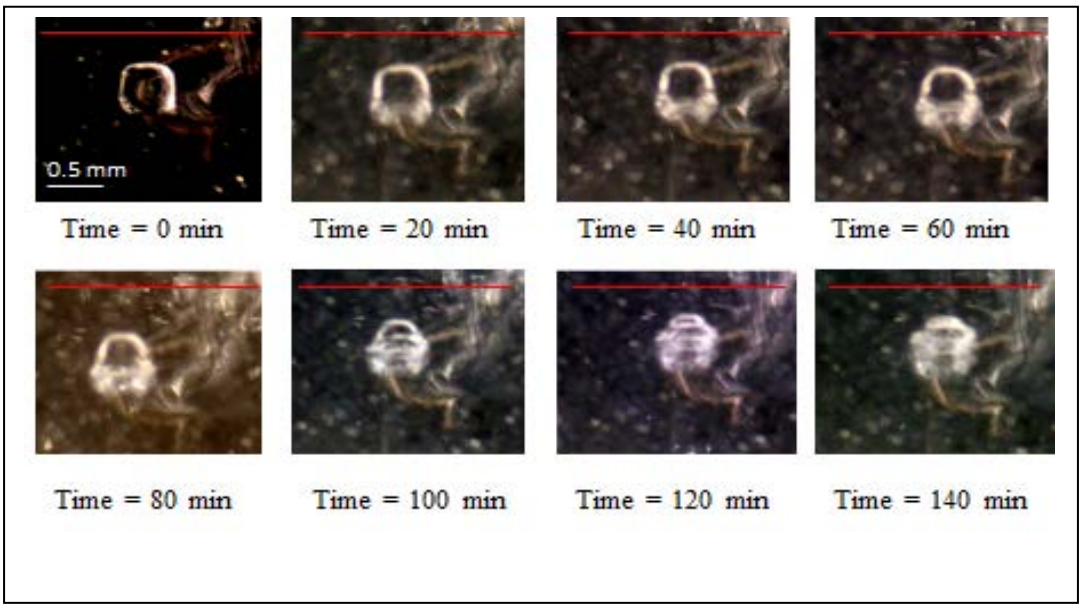

Figure 37. Still images showing the evolution of the shape of full brine inclusion in a thermal gradient. Temperature at the heating element is 200 ^{o}C.

The images show that the shape of the inclusion evolves from a square shaped inclusion with defined edges to a larger shape with more defuse edges. Following this initial transformation the inclusions migrate with a steady rate until they get within few millimeters of to the heat source (Figure 38).

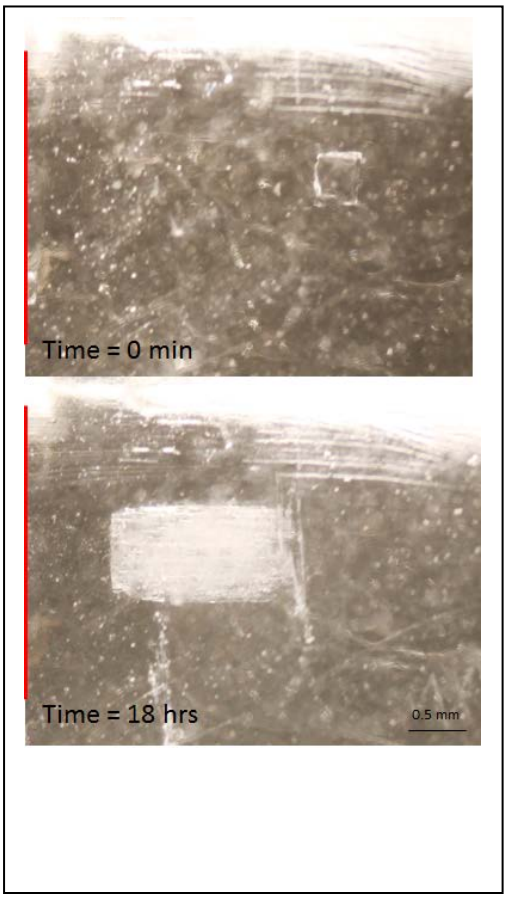

Figure 38. Still images showing the evolution of a single phase brine inclusion in a thermal gradient during a steady state migration. The top image was taken at the start of the heating and the bottom image was taken after 18 hours. Temperature at the heating element is 200 oC and temperature at the dissolution front varied during the experiment. Red line indicates the direction of the heat source

During the steady state migration the inclusions adopt a rectangular prism shape and with a well-defined edge on the hot side of the salt (left) and a more defuse side on the colder side of the inclusion (right). The migration path is only visible for a couple of millimeters near the inclusion and the original position of the inclusions are no longer visible following the migration. Figure 39 shows two images of a salt crystal

at time zero and the same salt crystal following 18 hours of heating. The image shows that the initial positions of the brine inclusions cannot be located during intermediate heating.

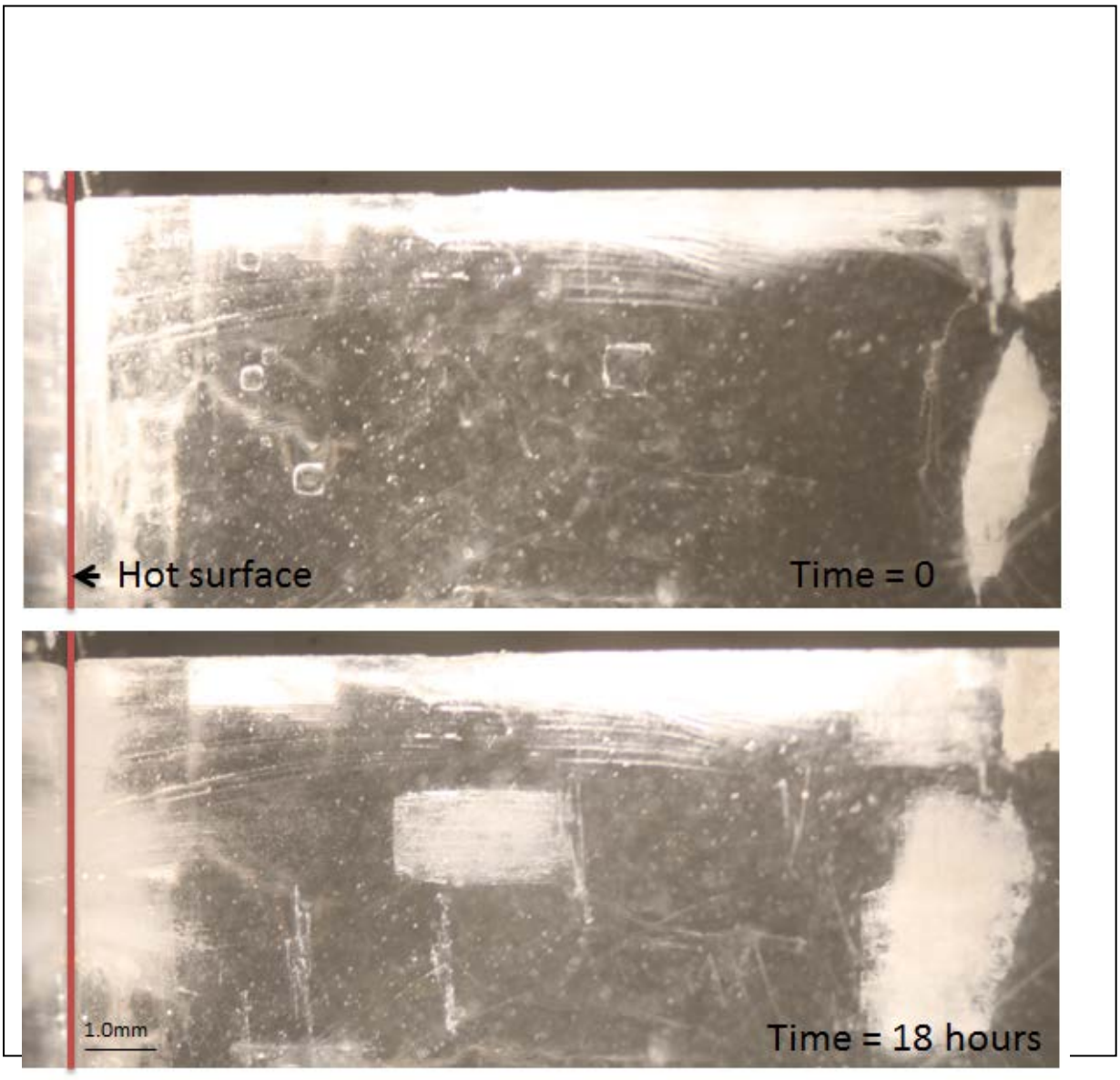

Figure 39. Still images showing the evolution of several brine inclusions over an extended heating time. Top image was recorded at the start of the heating and the bottom image at following 18 hours of heating. The temperature of the heating element was constant at 200 ^{o}C.

The image also shows that salt near the heating element is more opaque than that at the start of the experiment. A close up view of the brine migration pathway by microscopy shows the presence of granular species and appears to contain tiny arc shaped channels. Several of these arc shaped markings can be seen at the top of the bottom picture. Brine inclusions near the hot surface in the highly opaque section of the salt crystal (last couple of mm) migrate significantly faster than during the steady state stage. During this last stage brine exits the salt crystal rapidly.

3.3.2 Two phase (liquid / gas) inclusion migration in a thermal gradient

For studies of two-phase inclusions we selected salt crystals that contained both single phase and two phase inclusions. We heated one side of the salt crystal to a constant temperature and let the salt equilibrate. Temperatures of 60, 80, 100, and 200 ^{o}C for different durations were selected for the experiments. Under the influence of a thermal gradient the two phase inclusions undergo three stages of transformation. The first stage consist of the gas bubble within the inclusion moving away from the heat source (down the temperature gradient) while the brine itself moving towards the heat source (up the temperature gradient). The series of still images shown in Figure 40 show the evolution of a brine inclusion under a temperature gradient to 60 ^{o}C.

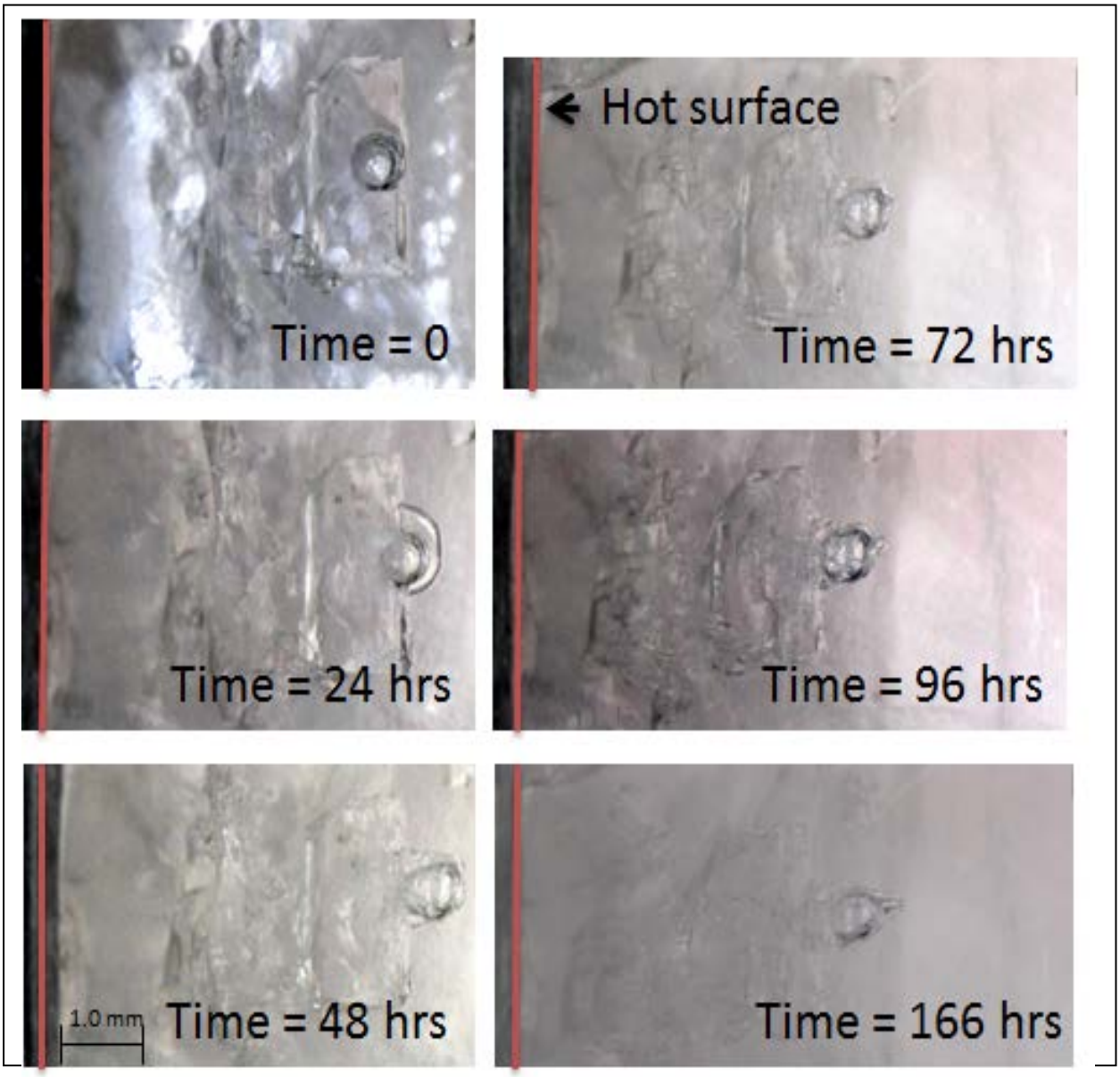

Figure 40. Still images showing the initial stage of two phase inclusions evolution under heat gradient. The temperature of the heating element was constant at 60 ^{o}C.

The images show that the initial gas bubble present in the inclusion moves down the thermal gradient and slowly etches a channel moving towards the cooler side of the salt (0 to 48 hours). Following this initial transformation, the gas bubble void created transforms into a thinner channel and continues to move down the thermal gradient (Figure 41 and 42). These images also show the evolution of brine (inclusion in the middle of the image), which slowly moves towards the heat source. When the brine reaches the hot

surface and releases through the fractured salt, the behavior of the gas bubble evolves rapidly. Narrow migration channels start to evolve from the cooler side of the inclusion and migrate rapidly towards the cold side of the salt crystal (Figure 42)

Figure 41. Images showing the migration of the gas phase to the cooler side of the salt crystal through narrow migration channels. Temperature at the hot end of the salt is 80 ^{o}C initially and then increased to 100 ^{o}C. Temperature at the cooler side is as indicated on the images.

Liquid migration in the two-phase inclusions behaves similar to that of single phase inclusions. The liquid phase moves towards the heat source in which the inclusion undergoes a shape change followed by a steady state migration (Figures 40, 41, 42).

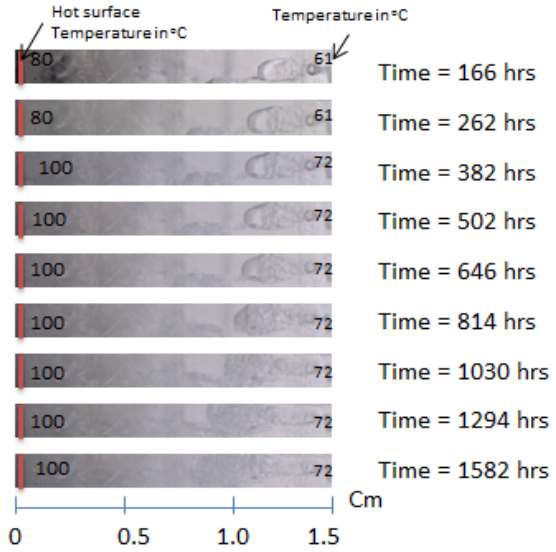

Figure 42. Images showing the migration of a two phase inclusion in a thermal gradient. The images depict the evolution of the inclusion on the right side of the pictures over time.

3.3.3 Mechanism of brine migration

Most of the past brine migration studies used high purity synthetic crystalline salt and used a controlled linear temperature gradient (Olander, 1981 a and b, Roedder, 1980). They found that single phase inclusions migrate up the temperature gradient and two-phase inclusion move down the temperature gradient. Single phase inclusions migrate by dissolution of the salt at the hot face of the inclusion and salt precipitation on the cold side of the inclusion. The transport of the salt through the cavity is defined by the molecular dissolution of the salt at the hot face of the inclusion and its diffusion to the cold side of the inclusion. The mechanism of two phase inclusion migration described in past studies involves the evaporation of brine at the hot face of the inclusion and its transport through the inclusion and

condensation on the colder side of the inclusion. The condensed water dissolves fresh salt on the cold side of the inclusion, thus moving the inclusion away from the heat source.

In our examinations we used natural polycrystalline salt, which has more impurities and is

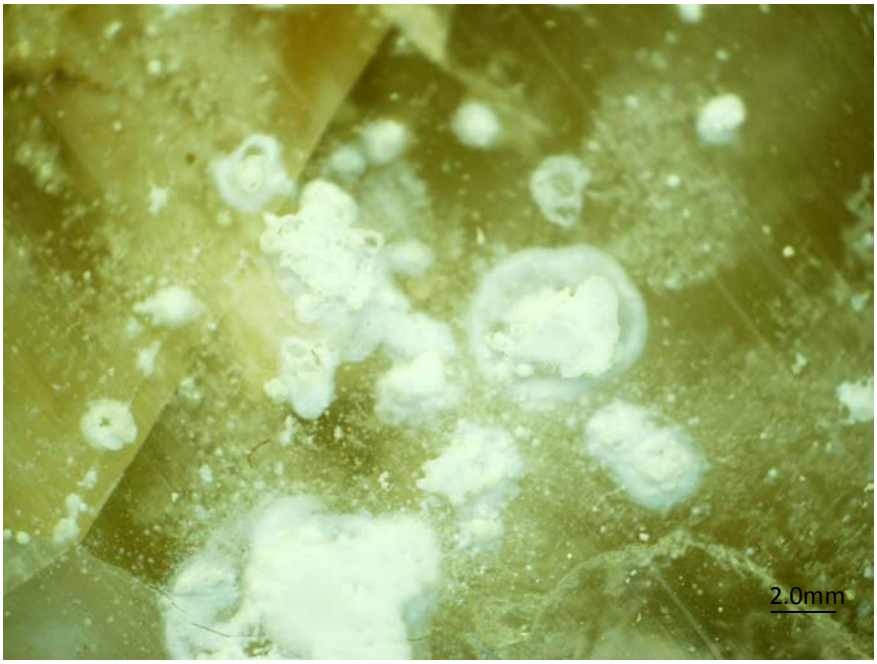

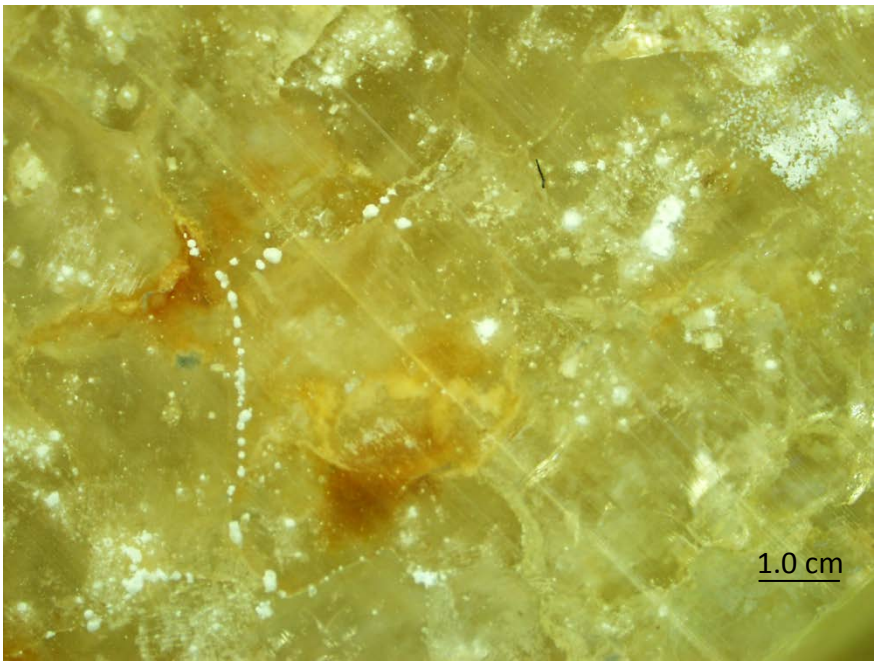

Figure 43. Photograph of the hot face of a polycrystalline salt sample heated to 200 ^{o}C for 3 weeks.. Note trace of efflorescence along crystal boundary, marking brine release from sample.

expected to have more crystalline defects. We subjected several samples to extended heating under applied thermal gradient. The samples contained both single phase and two phase inclusions. Following the heating experiment, selected samples were sectioned both parallel and perpendicular to the brine migration path and mounted for analyses by optical microscopy and SEM-EDS. We also performed elemental analysis of the salt precipitated along the migration channels and at the surface near the heating stage. These analyses were very useful in providing an understanding of the salt dissolution and migration mechanism. The optical images in Figure 43 show select photographs of the heated surface of polycrystalline salt samples heated at 200 ^{o}C. The photographs show that brine was released both at the salt grain boundaries and though the face of intact salt crystals. The deposited salt does not contain any of the impurities contained in the salt. Analyses by SEM/EDS confirm that salt deposited at the heated surface of the salt is pure sodium chloride. Analyses of the salt by SEM reveals that brine in both single phase and two phase inclusions migrates by creation of square shaped hollow migration channels. SEM images shown in Figure 44 show a salt crystal sectioned perpendicular to original location of a brine inclusion. The picture shows that brine migration does not dissolve the entire hot face of the inclusion. Brine migration operates through a mechanism that involves the creation of a network of channels that move up and down the temperature gradient. Full inclusions move exclusively up the temperature gradient when their temperature is not sufficiently high to create a gas phase. However, when the inclusions approach the hot surface, the high temperature induces the formation of a gas phase that moves away from the heat source. Following the creation of a gas phase, a dissolution front which moves down the thermal gradient is created and drives part of the moisture away from the heat source. The two phase inclusions moves in both directions with liquid brine moving up the temperature gradient while the gas phase moves down the temperature gradient. Dissolved salt is carried towards the heat source and is

deposited along crystal defects and irregular edges created along the migration channels (Figure 43). The composition of the salt deposited along the migration channels is enriched in NaCl. Elemental analyses of the salt deposited at the surface of fractured salt crystals in which no significant migration has occurred has significant amounts of $MgCl_2$, $CaCl_2$, and many other trace elements. It also shows the presence of crystalline SiO_2 (Figure 46). This is in agreement with past examinations of brine composition in the WIPP salt inclusions, which are rich in Mg and Ca. However, the presence of silicate materials has not been reported in the past. The elemental composition of the salt that has migrated minimally ~ few millimeters shows a significant reduction of Mg^{2+} and Ca^{2+} presence and complete absence of Mg^{2+} and Ca^{2+} in the salt deposited from inclusions that have migrated to the surface up the temperature gradient. EDS analyses show that migrated salt is pure NaCl.

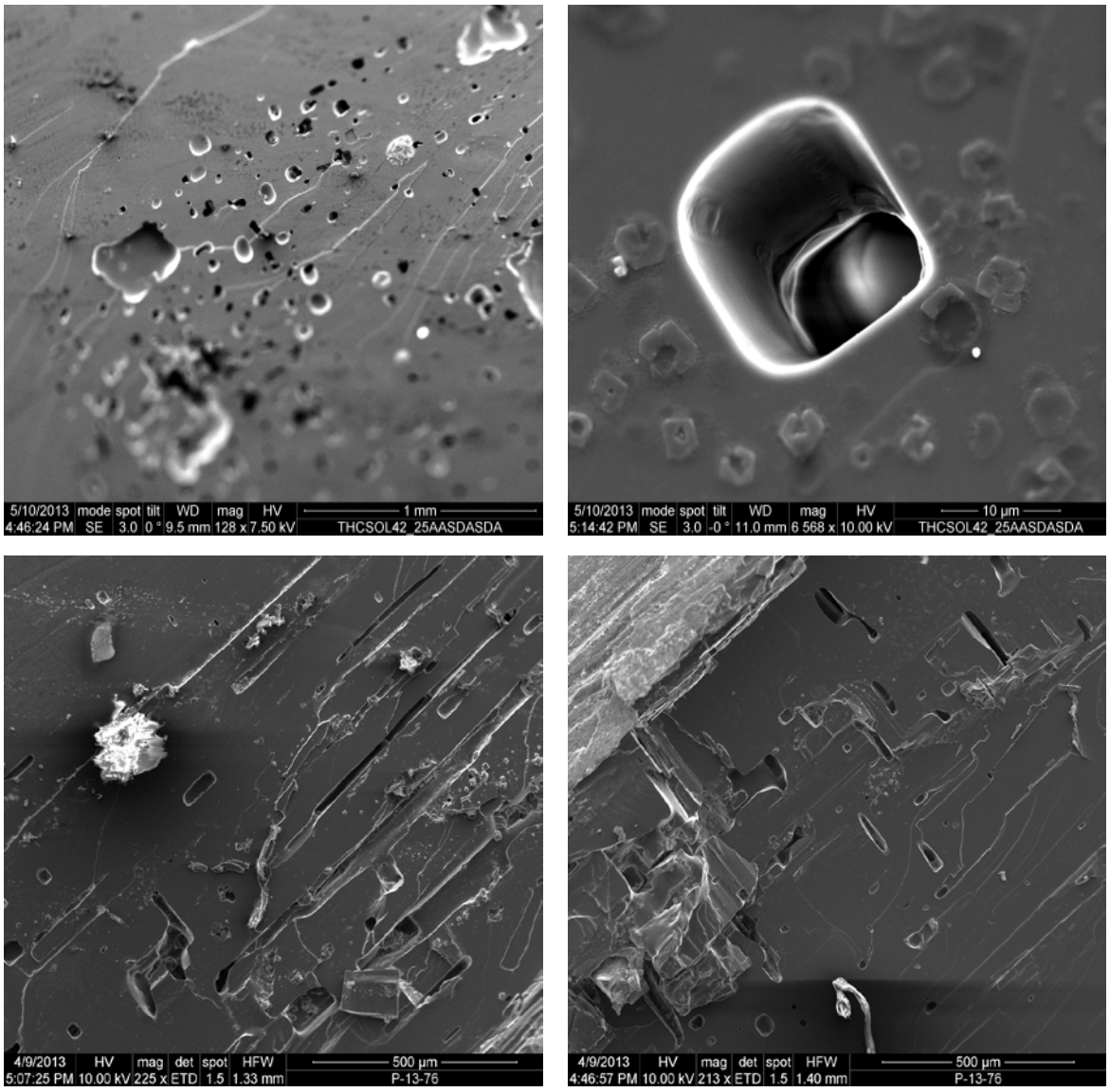

Figure 44. SEM images of inclusion pathways in salt crystals. Top row shows samples sectioned perpendicular to the migration channels, enlarged photo in upper right. Bottom row images depict brine transport tubules parallel to migration pathway.

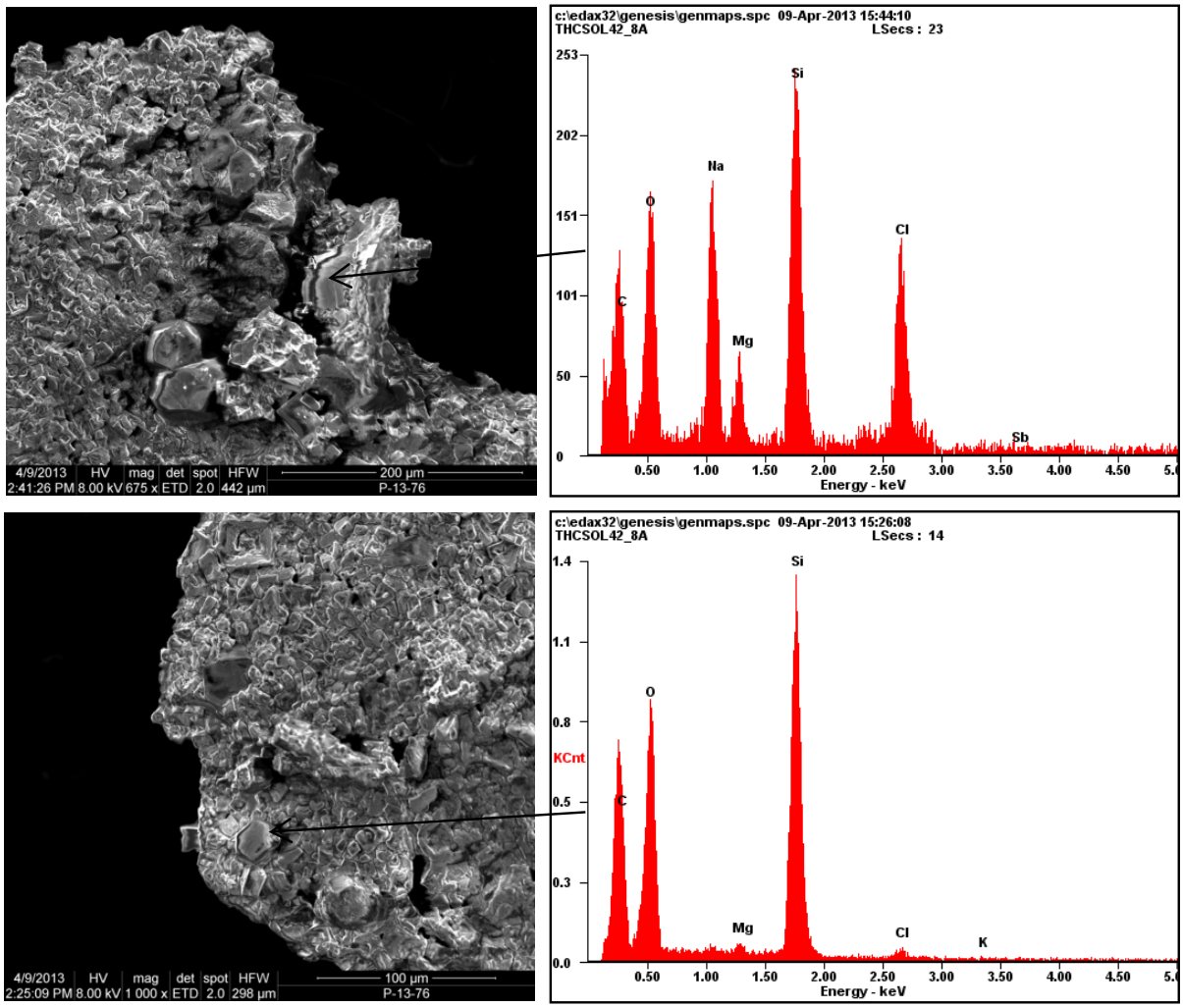

Figure 45. SEM images of salt efflorescences deposited at the surface from a brine inclusion that burst following heating. EDS analysis shows elemental analysis of the deposited salt which reflects a brine composition that is rich in silicate and other elements. Crystalline silicate particles are abundant in the salt deposited and are identified as detrital quartz.

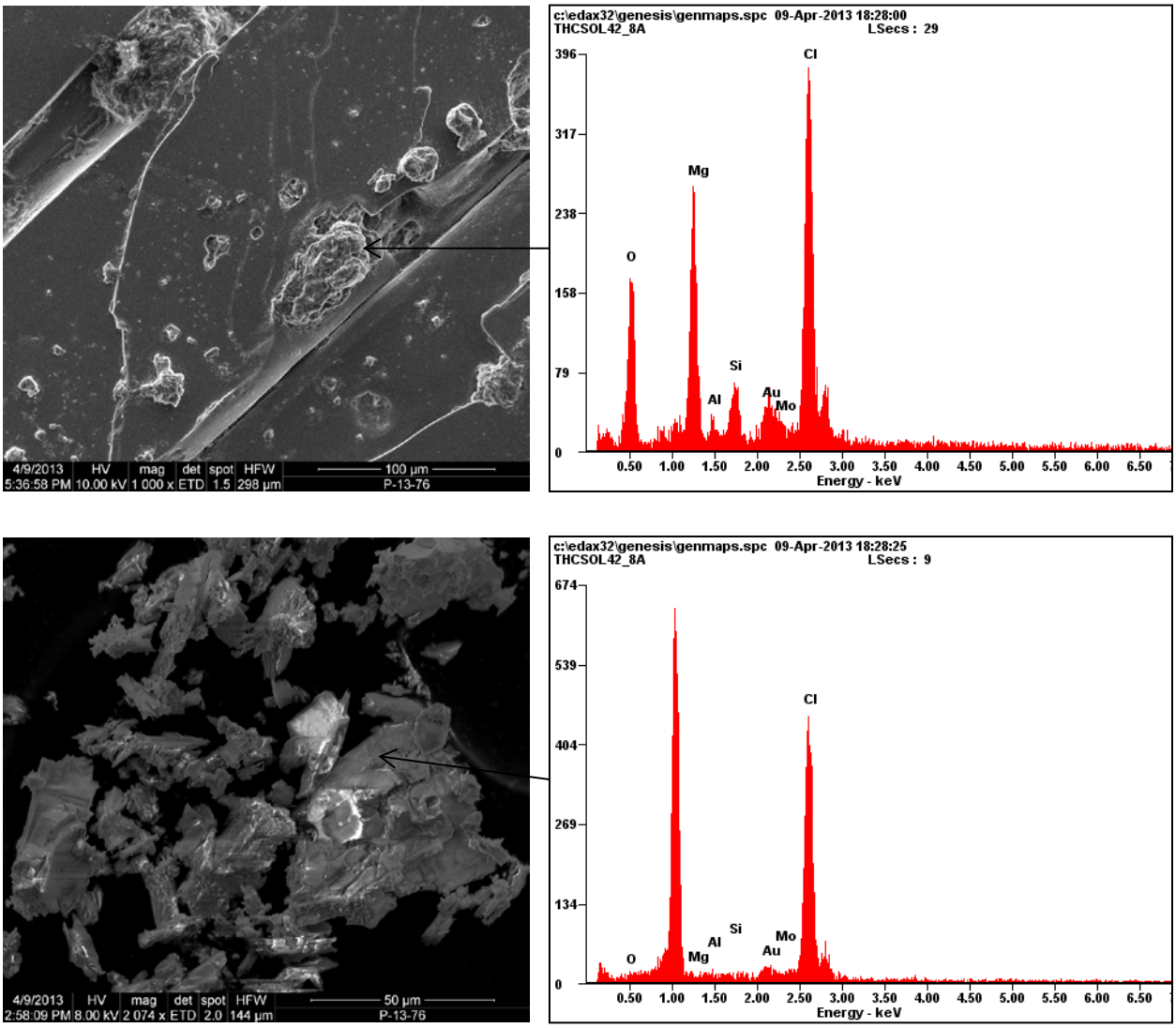

Figure 46. SEM and EDS analysis of precipitated salt deposited along the migration path (top) and salt deposited at the end of the migration path in contact with the heat source (bottom).

SEM analyses of the brine migration pathway and the composition of the deposited salt are very informative. They reveal that salt dissolution at the hot face of the inclusion proceeds through a network of dissolution channels that create a porous media for water to travel through. The deposition of NaCl crystallites along the migration pathways indicates that dissolved salt at the hot face of the inclusion moves down the thermal gradient (creating over saturated brine). The subsequent precipitation of the salt therefore changes the composition of the original brine.

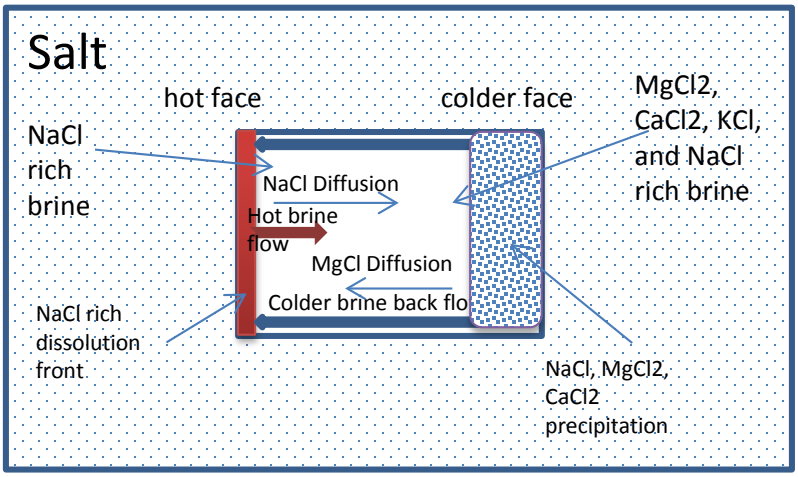

Figure 47. Schematic representation of the mechanisms of brine migration under thermal gradient.

The mechanism of thermally induced single phase inclusions migration is illustrated in the Figure 47. Salt is dissolved at the hot face of the inclusion because of the increased solubility of salt due to temperature increase. The dissolution front is composed of brine saturated with NaCl and is hotter than the remaining brine in the inclusion, whichinitially is composed of $MgCl_2$, NaCl, KCl and other elements. The difference in temperature and chemical composition between the dissolution front and the remaining inclusion will set up a convection cell. The cell creates a flow of hot brine towards the colder face of the inclusion and a flow back of colder brine towards the hot face of the inclusion. As a result of these flow conditions, unsaturated brine will be continually supplied to the hot side of the inclusion and over saturated brine will be transported to the colder side of the inclusion. These flow processes and chemical conditions provide the mechanism which drives the salt dissolution and precipitation. The series of images shown in Figure 37 show that the inclusions change shape progressively at the colder side of the inclusion as a result of salt precipitation. The dissolving front of the inclusion is composed of pure NaCl while the original brine has $MgCl_2$, $CaCl_2$, KCl and other trace elements. As a result of the slow diffusion of the cations in this closed system, the liquid brine will become enriched with NaCl as the brine migrates towards the heat source. This is supported by the elemental composition analysis of deposited salt in

Figure 46, which shows migrated brine becomes enriched in NaCl, while salt precipitated at the start of the migration is more Mg^{2+}, Ca^{2+}, K^{+} rich in composition.

Based on this analysis of the migration path (Figures 46 and 47), it is clear that the parameters that will play a significant role in brine migration under thermal gradients are 1)the temperature of the hot face of the inclusion, 2) the magnitude of the thermal gradient across the inclusion (which influences the speed of the brine flow and the dissolution/precipitation of the salt), 3)the presence of defects and impurities in the salt, and 4) the ratio between the size of the inclusion and the dissolving front.

3.3.4 Rate of Brine migration

The rate of brine migration in single salt crystals varied as a function of the inclusions position relative to the heat source and the temperature gradient established in the salt. The data shown in Figure 48 show an example of the migration velocities typically obtained from our experiments. The data show that the size of the inclusions has very little influence on the rate of brine migration. It is also apparent from the data that brine migration rate is enhanced as the inclusions get closer to the heat source. This is due to the increase in both the temperature at the dissolving front (hot face of the inclusion) and the increase of the temperature gradient established within the brine inclusion. The data show that the temperature of the hot face of the inclusion and the amplitude of the temperature gradient are the most important parameters that influence the velocity of brine migration.

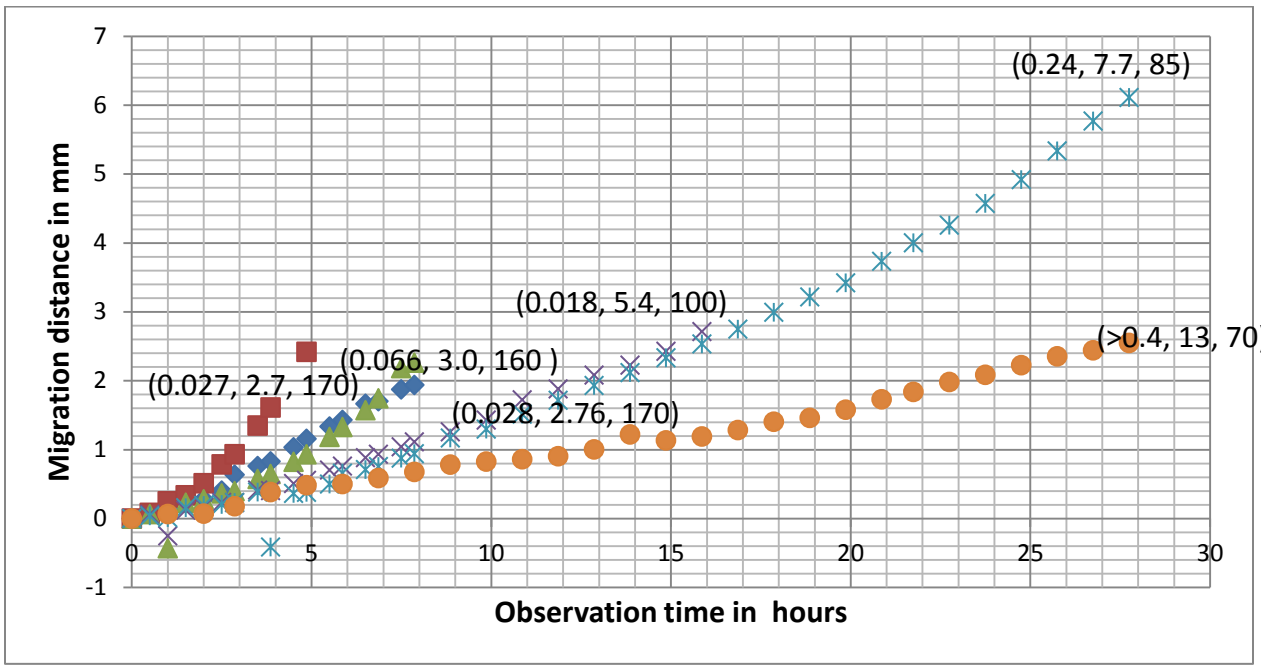

Figure 48. Plot of brine inclusions migration distance in a single crystal as function of time. The temperature at the hot face of salt was fixed at 250 ^{o}C. Numbers in parentheses (a, b, c) represent a) the volume of the inclusion (mm^3), b) the distance from the heating source, and c) the temperature of the hot face of the inclusion at the start of the experiment, respectively..

The analytical equations describing the migration of inclusions within the body of a salt crystal developed

in past studies (Jens, 1979; Anthony,1971; Anthony,1972) and is given by the following equation:

$$V = \frac{C_l}{C_s}\frac{D}{RT}\left[\left(\frac{1}{C_l}\frac{\partial C_E}{\partial T} - \sigma\right)G_l RT - \frac{K}{L} - \frac{4\gamma \bar{V}_s}{XL}\right]$$

Where V = migration velocity in cm/sec

Cl= concentration of salt in brine inclusion in moles/liter

CE= equilibrium concentration of salt in brine in contact with salt in moles/liter

Cs concentration of salt in solid salt in moles/liter

D diffusivity of salt in brine in cm^2/sec

R = diffusivity of salt in brine in Cm^2/sec

R = gas constant in erg mole-1 C-1

T = absolute temperature in ^{o}K

K = kinetic potential in ergs/mole

Y = grain boundary tension in ergs/cm^2

Application of this analytical equation does not fit our brine migration data. The temperature gradient applied during our experiments is not linear making it more difficult to apply this model. In addition, our experimental results do indicate that salt diffusion has a very limited influence on the overall rate of brine migration. We believe that the migration rate is more closely related to the rate of fluid transport in the convection cell established within the inclusion. Efforts are underway to develop an alternative model for the prediction of brine inclusions migration based on nonlinear temperature gradient and a dissolution rate driven by a convection cell within the brine inclusions.

4. CONCLUSIONS

The amount of water released from salt was found to be linearly correlated to the rock's accessory mineral content (Deal, et al, 1989). This is a critical parameter that has been mostly avoided in previous salt repository modeling studies. However, it is not clear how the water released from these secondary minerals will behave in a thermal gradient. Experimental studies were therefore required to determine the water behavior released from secondary minerals in a thermal gradient and how the water migrates in the salt beds.

The results from this study on brine migration in salt indicates that the water content in salt is mainly controlled by the hydrous mineral content, and to a lesser extent, salt brine inclusions. . Experiments have provided strong evidence of mineral dehydration at 65-75^{o}C for both clays and sulfates. The corrensite (clay) loss of interlayer water releases 5 to 13 wt% over a short temperature span of 10 degrees. Over that same temperature range (65-75^{o}C) the gypsum to bassanite phase transformation releases 15 wt% water.

We have also determined further dehydration of both mineral groups at higher temperatures, however these high temperature results are preliminary in nature. Robertson and Bish (2013) have concluded that RH is critical to sulfate stability. This parameter has not yet been fully determined for salt repository conditions. There is also a need to perform sulfate stability experiments to determine the temperature, RH, and pressure constraints concerning the 1stage (gypsum to anhydrite) vs. 2 stage (gypsum to bassanite to anhydrite) phase transformations.

Stein (1985) described the stratigraphy at WIPP in the repository horizon, however we have found significant mineralogic proportion differences. Further field examinations and sample collection are required to establish a more accurate description of the proportion of hydrous minerals in salt beds . This will further define the water content in rock salt, how it is correlated to accessory hydrous minerals present in salt, and the mechanisms by which water will be released in a higher thermal heat load environment.

Results from this study also illustrate the high porosity of crushed salt (0.39 +- 0.02) and the low thermal conductivity of salt. This study demonstrated the low coupling between the heat source and salt which results in the immediate drop of temperature in the salt in contact with a heating source. The thermal gradients established within the heated salt are strongly dependent on the heat load. Very large thermal gradients of up to 50 ^{o}C/cm are observed when the temperature of the heat source is near 200 ^{o}C. Much lower thermal gradients (20 to 30 ^{o}C/cm) are observed at lower temperatures. Thermal gradients in crushed salt vary exponentially with the distance from the heat source and range between 50 and 10 ^{o}C/cm.

The single crystal brine migration studies performed in this investigation show that brine inclusions move up the thermal gradient independent of whether they are single phase (liquid) or two phase (liquid and gas). We also found that all inclusions become two-phase inclusions when they near the heat source. The gas phase in the two-phase inclusions moves away from the thermal source. The brine migration

mechanism involved the dissolution of salt at the hot face of the inclusion and its deposition at the colder side of the inclusion. This process is driven by convective flow that drives unsaturated/cold brine to the hot face of the inclusion and over saturated/hot brine towards the colder side of the inclusion. Salt dissolution within a brine inclusion creates a network of square shaped 10 um migration channels parallel to the thermal gradient. The salt precipitated becomes enriched in NaCl as the salt migrates towards the heat source.

In light of the research performed in FY 13, there is a natural progression to better understand mineral dehydration mechanisms and brine migration in multi-crystal salt rocks. Outlined below in bullet form are specific lines of research that will 1) address multiple variables in the dehydration trigger mechanisms for clay and sulfates, and 2) allow for studies of brine migration in salt at the next larger scale (multi crystalline in a core sized sample).

Hydrous mineral research - FY-14

- Sample collection and quantitative determination of hydrous minerals in salt and water content in salt.
- Clay hydration / dehydration at 75 ^{o}C
- Sulfate phase transformations (75 – 275 ^{o}C) – one vs. two step (stability of bassanite)
- Effect of RH on sulfate stability
- Mobility of hydrous phase water liberation in intact rock (core size samples)

Salt brine migration research – FY14

Focus on core samples to provide data concerning scaling issues:

- Develop a brine inclusions migration model based on brine convective flow of brine within the inclusions and compare to existing models.

- Confirm thermal conductivity results from the single crystal study,
- Determine and characterize brine movement in a solid, multigrain rock,
- Provide a fluid transport mechanism to enhance present day Thermo Mechanical modeling

5. REFERENCES

Anthony, T.R. and Cline, H.E. 1971 " The thermomigration of liquid Droplets through solids" J. Appl. Phys. V42, pp 3380.

Anthony, T.R. and Cline, H.E. 1972 " The thermomigration of biphase Vapor-liquid droplets in solids" Acta Metall. V20, pp 247.

Altaner, S.P., and Ylagan, R.F. 1997 "Comparison of Structural Models of Mixed-Layer Illite-Smectite and Reaction Mechanisms of Smectite Illitization." Clays and Clay Min., V45, pp 517-533.

Bein, A; Hovorka, S.D.; Fisher, R.S.; Rodder E. 1991 "Fluid inclusions in bedded Permian halite, Palo Duro, Basin, Texas- Evidence for modification of seawater in evaporate Brine-pools and subsequent early diagenisis" Journal of Sedimentary Petrology, V61(1): pp 1-14.

Bradshaw, R.L. and W.C. McClain, Eds. 1971. "Project Salt Vault: A Demonstration of the Disposal of High-Activity Solidified Wastes in Underground Salt Mines." ORNL-4555. Oak Ridge, TN: Oak Ridge National Laboratory.

Braitsch, O, 1971 "Salt deposits their origin and composition" Springer-Verlag, New York, 297pp.

Brush, L.H. 2012. "Review of Brines, Brine Chemistry, and Brine Migration in a Salt Repository for Spent Fuel or HLW" Sandia National Laboratory.

Brush, L.H. 1990. "Test Plan for Laboratory and Modeling Studies of Repository and Radionuclide Chemistry for the Waste isolation Pilot Plant". SAND90-0266. Albuquerque, NM: Sandia National Laboratories.

Chipera, S.J. and Bish, D.L. (2002) FULLPAT: a full-pattern quantitative analysis program for X-ray powder diffraction using measured and calculated patterns. Journal of Applied Crystallography, V35, pp 744–749.

D'Ans, J., Bredtschneider, D., Eick. H., & Freund, H. E., 1955. Untersuchungen iiber die Calciumsulfate. *Kali und Steinsalz* (S:r. 1), Heft V9, pp 17-38.

Deal, D.E., and R. J. Abitz, D. S.Belski, J.B.Case, M.E. Crawley , R.M. Deshler, P.E. Drez,C.A. Givens, R.B. King, B.A. Lauctes, J. Myers, S. Niou, J.M. Peitz, W.M. Roggenthen, J.R. Tyburski, and M. G. Wallace, 1989. Brine Sampling and Evaluation Program, 1988 Report, DOEJWIPP 89-015, Section 4.1.

DOE/WIPP 02-3177, Volume 1, Geotechnical Analysis Report for July 2000–June 2001 September 2002.

Dosch, R.G. 1976. "Analytical Work in Development of Synthetic Brine Compositions." Memorandum to M.A. Molecke, October 12, 1976. Albuquerque, NM: Sandia National Laboratories.

Ferrage, E., Vidal, O., Mosser-Ruck, R., Cathelineau, M., and Cuadros, J. (2011) A reinvestigation of smectite illitization in experimental hydrothermal conditions: Results from X-ray diffraction and transmission electron microscopy. Am. Min., V96, pp 207-223.

Freyer,D. 2000 Zur Phasenbildung und stabilitat im System Na_2SO_4 – $CaSO_4$ – H_2O. Dissertation , TU Bergakademie, Feiburg.

Freyer, D. and Voigt, W. (2003) Invited Review: Crystallization and Phase Stability of $CaSO_4$ and $CaSO_4$-Based Salts. Mon. fur Chemie V134, pp 693-719

Greenburg, H.R. and Wen, J. (2013) Repository layout and host rock thermal gradient trade study for large waste packages in clay/shale: Using the DSEF thermal analytical model. LLNL-TR-639869-DRAFT, pp. 38.

Hardie, L.A., 1967, The gypsum-anhydrite equilibrium at one atmosphere pressure. Am Min, V52, pp 171- 200.

Jens, G. H. 1979, " Effect of temperature, temperature gradients, stress, and irradiation on migration of brine inclusions in salt repository" ORNL-5526.

Hohlfelder, J.J., 1979, " Measurement of water loss from Heated Geologic salt". SAND79-0462. Albuquerque, NM: Sandia National Laboratories.

Hohlfelder, J.J., 1981, "Volatile content of rock salt". SAND79-2349. Albuquerque, NM: Sandia National Laboratories.

Hohlfelder, J.J., McMurtry 1982, "Water content of brines contained in southeast New Mexico rock salt". SAND82-0530. Albuquerque, NM: Sandia National Laboratories.

Huang, W.L.; Bassett, W. and Wu, T. 1994"dehydration and hydration of montmorilonite at elevated temperature and pressures monitored using synchrotron radiation". Am. Min. V79, pp 683-691.

Krause, W.B. 1983. "Avery Island Brine Migration Tests: Installation, Operation, Data Collection, and Analysis." ONWI-190(4). Columbus, Ohio: Battelle Project Management Division, Office of Nuclear Waste Isolation.

Krumgalz, B.S., Starinsky, A., Pitzer, K.S. (1999) Ion-interaction approach: Pressure effect on the solubility on some minerals in submarine brines and seawater. J. Soln. Chem, 28, pp 667-692

Krumhansl, J.L., Kimball, K. M. and Stein, C.L. 1990, "A review of WIPP repository Clays and their relationship to Clays of adjacent strata" SAN-90-0549. Sandia, National, Laboratory, Albuquerque, NM.

Kopp, O. C., and Combs, D. W., 1975, "Mineral sources of water in evaporite sequences (Salado salt and adjacent beds at the proposed waste disposal facility near Carlsbad in Lea and Eddy Counties, New Mexico)". Oak Ridge National Laboratory, Final Report, ORNL/SUB-3670-3-4, 34 pp.

Line C.M.B. and Kearley G.J., 2000, An inelastic incoherent neutron scattering study of water in small-pored zeolites and other water-bearing minerals, J. Chem. Phy., V112 (20), pp 9058-9067.

Lippmann, F. (1976) “Corrensite, a swelling clay mineral, and its influence on floor heave in tunnels in the Keuper Formation”. Eng. Geol., V 13, pp 65-70.

Machiels, A.J.; Yagnik, S.; Olander, D.R.; Kohli, and R. 1981, “The mechanism of intragranular migration of brine inclusions in salt” Transaction of the American Nuclear Society, V38: pp 169-170.

Molecke, M.A. 1983. *A Comparison of Brines Relevant to Nuclear Waste Experimentation.* SAND83-0516. Albuquerque, NM: Sandia National Laboratories.

Monnin, C. 1990 The influence of pressure on the activity coefficients of the solutes and on the solubility of minerals in the system Na-Ca-Cl-SO_4-H_2O to 200°C and 1 kbar and to high NaCl concentration. Geochim Cosmochim Acta, V54, pp 3265-3282

Monnin, C. 1999 A thermodynamic model for the solubility of barite and celestite in electrolyte solutions and seawater to 200°C and to 1 kbar. Chem Geol, V153, pp 187-209

Nowak, E.J., and D.F. McTigue. 1987. “Interim Results of Brine Transport Studies in the Waste Isolation Pilot Plant (WIPP).” SAND87-0880. Albuquerque, NM: Sandia National Laboratories.

Nowak, E.J. 1986. “Preliminary Results of Brine Migration Studies in the Waste Isolation Pilot Plant (WIPP).” SAND86-0720. Albuquerque, NM: Sandia National Laboratories.

Olander, D.R.; Machiels, A.J.; Balooch, M.; Muchowski, E.; Yagnik, S.K.” Thermomigration of brine inclusions in sodium chloride single crystals” Trans. Am. Nucl. Soc.; 1980, V34: pp 352-353.

Olander, D.R.; Machiels, A.J.; Yagnik, S.K. 1981a, ”Thermomigration of two-phase inclusions in salt” Trans. Am. Nucl. Soc.;, V35: pp 168-169.

Olander, D.R.; Machiels, A.J.; Muchowski, E.1981b, “Migration of Gas-liquid inclusions in single crystals of potassium and sodium chlorides” Nuclear Science and Engeneering, V79 (2): pp 212-227.

Popielak, R.S., R.L. Beauheim, S.R. Black, W.E. Coons, C.T. Ellingson and R.L. Olsen., 1983, "Brine Reservoirs in the Castile Formation, Waste Isolation Pilot Plant Project, Southeastern New Mexico" TME 3153. Carlsbad, NM: U.S. Department of Energy WIPP Project Office.

Pusch, R (2008) Geological Storage of Radioactive Waste. Springer-Verlag, Berlin, Germany, pp. 379.

Robertson, K., and Bish, D. (2013) Constraints on the distribution of $CaSO_4$_nH_2O phases on Mars and implications for their contribution to the hydrological cycle. Icarus, V223, pp 407-417

Roedder, N. and Belkin H.E.,1980, "Migration of fluid inclusions in polycrystalline salt under thermal gradients", in Proc. of the 1980 NWS Progr. Info. Mtg., 0NWI-212, pp 361.

Roedder, E.; Bassett, R. L., 1981, "Problems in determination of the water content of rock-salt samples and its significance in nuclear-waste storage siting". *Geology*. V9 (11):pp 525-350.

Rothfuchs, T., K. Wieczorek, H.K. Feddersen, G. Staupendahl, A.J. Coyle, H. Kalia, and J. Eckert. 1988. "Brine Migration Test: Asse Salt Mine, Federal Republic of Germany. Final Report." GSF-Bericht 6/88. Munich, Germany: Society for Radiation and Environmental Research.

Ryan P.C., and Hillier, S. (2002) Berthierine/chamosite, corrensite, and discrete chlorite from evolved verdine and evaporite-associated facies in the Jurassic Sundance Formation, Wyoming. Am Min, V87, pp 1607-1615

Seyfried, J.R., Janecky, D.R., and Berndt, M.E. (1987) Rocking autoclaves for hydrothermal experiments II. The flexible reaction-cell system. Hydrothermal Experimental Techniques. Eds. Ulmer, G.C. and Barnes, H.L. John Wiley and Sons, pp. 216 - 239

Shcherban, J.P., and Shirokikh, I.N. (1971) Thermodynamic and experimental data on Stability of gypsum, hennhydrate, and anhydrite under hydrothermal conditions. Int. Geology Review, V13: (11), pp 1671-1673.

Shefelbine, H. C., 1982, “Brine migration in salt: A summary report”. SAND82-0152. Albuquerque, NM: Sandia National Laboratories.

Smyth, J.R., and Bish, D. 1988 "*Crystal Structures and Cation Sites of the Rock-Forming Minerals*" Allen & Unwin. 332 pp.

Snider, A.C. 2003. “Verification of the Definition of Generic Weep Brine and the Development of a Recipe for This Brine.” Analysis report, April 8, 2003. Carlsbad, NM: Sandia National Laboratories. ERMS 527505.

Stein, C. L., 1985, “Halite mineralogy in the WIPP facility stratigraphic horizon. SAND85-0321, Sandia, National, Laboratory, Albuquerque, NM. 32 p.

Stewart, F. H., 1963, “Marine evaporites: U.S. Geological Survey Professional Paper 440Y, 52 pp.

Stauffer, P.; Harp, D.; Robinson, A.B., Model Development and Analysis of the Fate and Transport of Water in a Salt-Based Repository, LANL Report LA-UR-12-25050.

Sugimoto, K., Dinnebier R. E. and Hanson J. C. 2007. “Structures of three dehydration products of bischofite from in situ synchrotron powder diffraction data (MgCl2·nH2O; n = 1, 2, 4)”. Acta Cryst. , V B63, pp 235-242

Velde, B. (1977) A proposed phase diagram for illite, expanding chlorite, corrensite and illite-montmorillonite mixed layered minerals. Clays Clay Min. V25, pp 264-270

Vidal, O., and Dubacq, B. (2009) Thermodynamic modeling of clay dehydration, stability and compositional evolution with temperature, pressure and H2O activity. Geo. Cosmo. Acta., V73, pp 6544-6564.

Wu, T.C., Bassett, W., Huang, W.L., Guggenheim, S., and Koster Van Groos, A.F. 1997 “Montmorillonite under High H_2O pressures: Stability of Hydrate Phases, Rehydration Hysteresis, and the Effect of Interlayer Cations.” Am. Min., V82, pp 69-78.

Yagnik, S.K. 1982 “Thermal gradient migration of brine inclusions in salt” Western Regional American Nuclear Society Student Conference, Oregon State University, Corvallis, OR, March 28-30, 1982. LNL-14080

Yagnik, S.K. 1983, “ Interfacial stability of migrating brine inclusions in alkal-i-halide single-crystals supporting a temperature-gradient” Journal of crystal Growth, V62 (3): pp 612-626.

Appendix A

Detailed characterization of salt dehydration studies performed by TGA

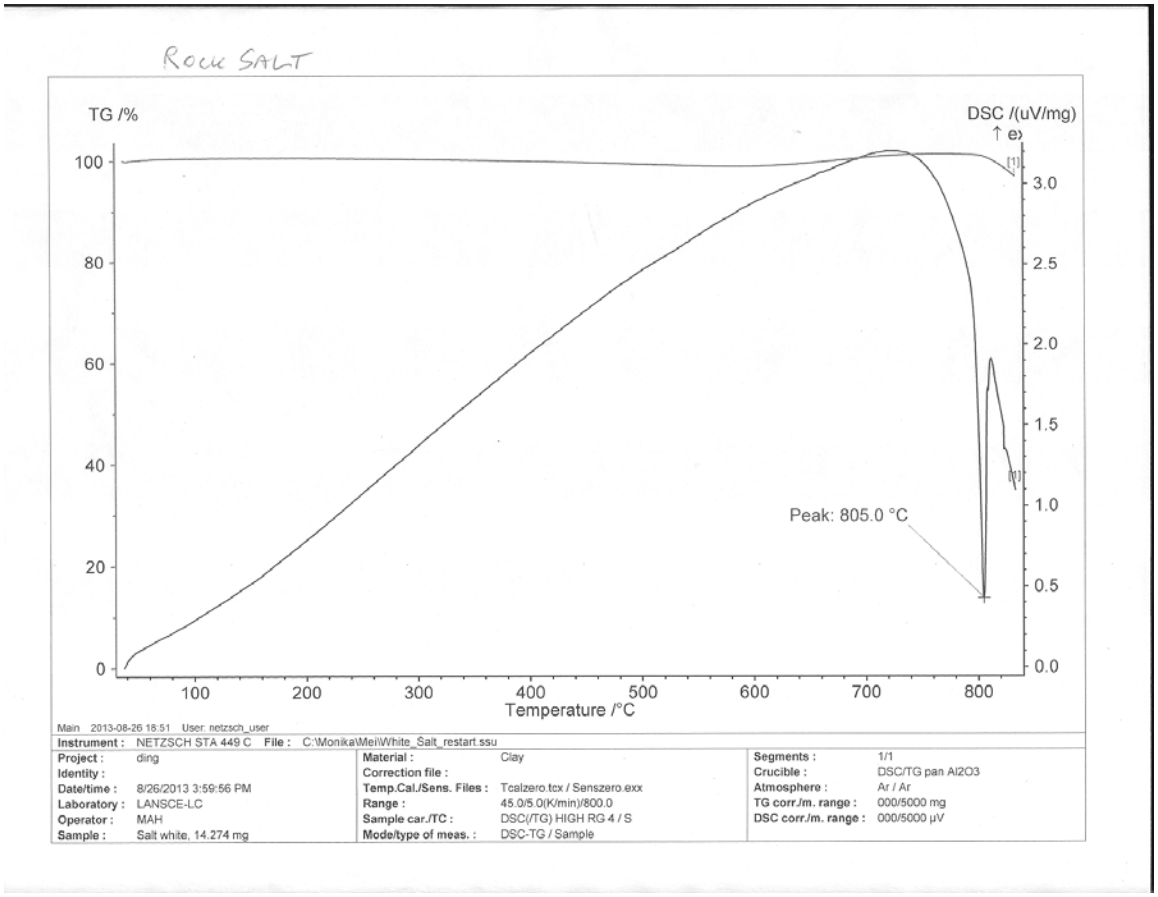

Figure A1. Raw TGA spectrum of sample 1 Rock Salt (White).

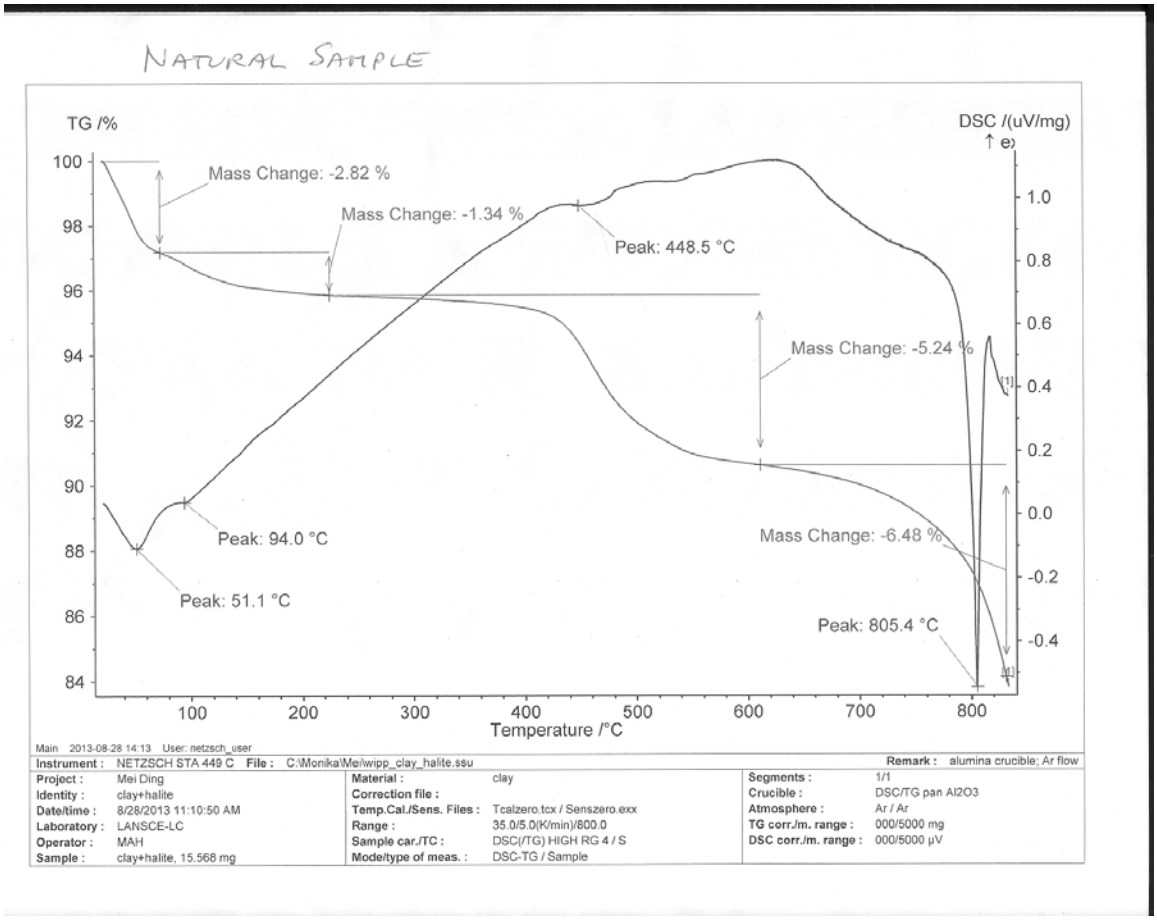

Figure A2. Raw TGA spectrum of sample 2, Rock salt/clay.

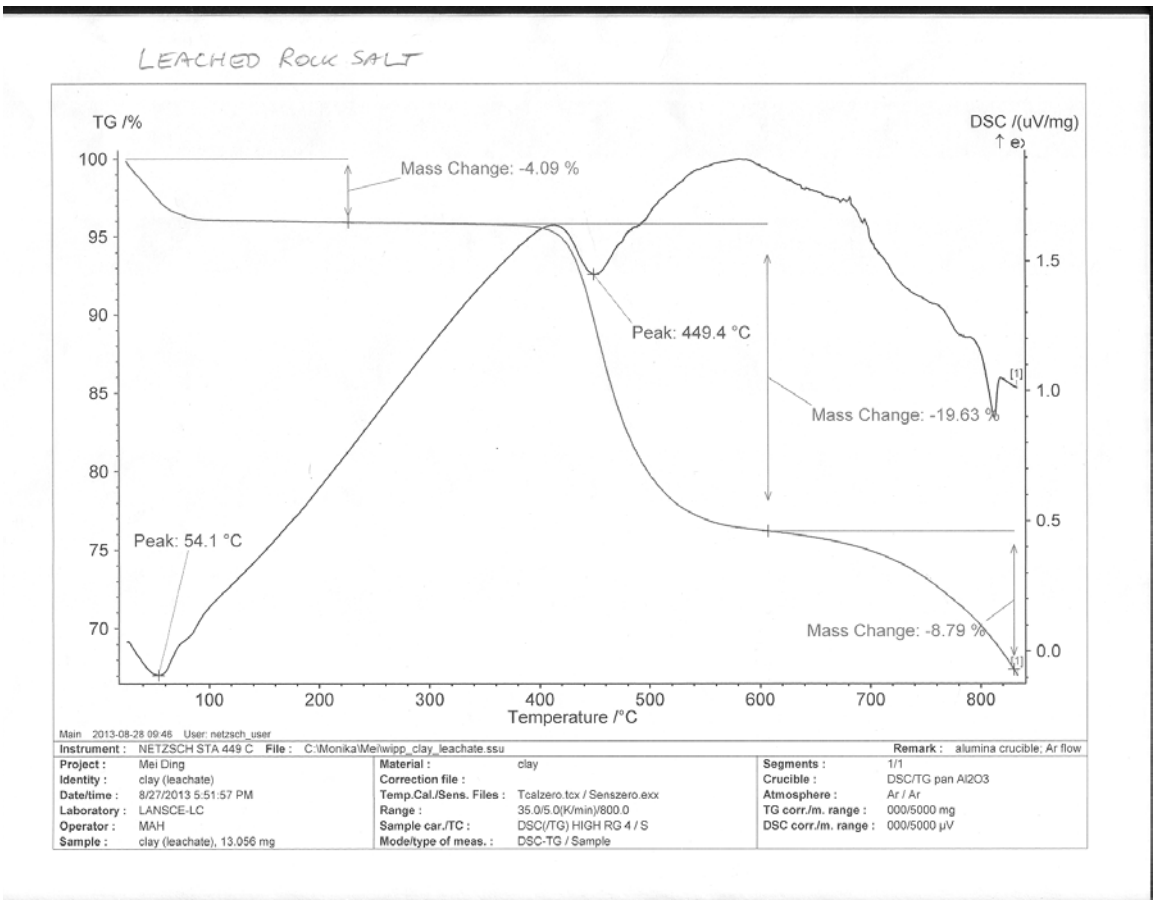

Figure A3. Raw TGA spectrum of sample 3, Leached rock salt/clay.

Detailed characterization of salt used in TGA and DFS experiments

Two Permian rock samples with a large difference in clay content and one leachate of larger clay content were selected in this study. We designated the sample appearing transparent with lesser clay content as rock salt: sample 1, the grey colored sample with higher clay content as sample 2, and the non salt leachate minerals of sample 2 as sample 3. Detailed sample description and characterization are listed in Table 1.

Table 1. Mineralogical composition of three samples used in the study

Samples	Sample Description	Mineral Content

1	*Rock Salt (White):* Clear color, completely transparent	Not determined
2	*Rock Salt/Clay:* Grey color, less transparent	Major: Halite (NaCl) Minor: Magnesite ($MgCO_3$)
3	*Leached Rock Salt/Clay:* Leachate of sample 2 with concentrated fraction of nonsalt minerals of sample 2	Major ; Smectite, Mica, Kaolinite Quartz, (SiO_2) Trace amont : Halite (NaCl), Magnesite ($MgCO_3$)

XRD (X-ray Diffraction) results of sample 2 and 3 are shown in Figure 1 and 2.

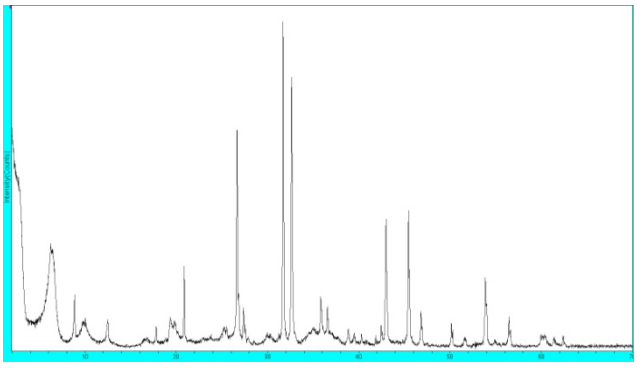

Figure 1. XRD for sample 2.

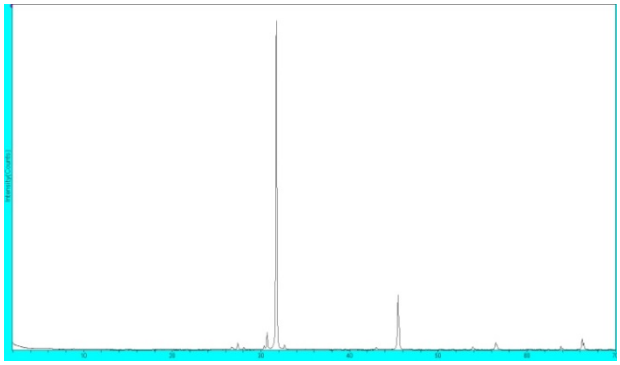

Figure 2. XRD for sample 3.